Macromolecules

pubs.acs.org/Macromolecules Article

Structure and Dynamics of Hybrid Colloid–Polyelectrolyte Coacervates

Artem M. Rumyantsev,* Oleg V. Borisov,* and Juan J. de Pablo*

Cite This: *Macromolecules* 2023, 56, 1713–1730

Read Online

ACCESS | Metrics & More | Article Recommendations

ABSTRACT: We develop a scaling theory for the structure and dynamics of "hybrid" complex coacervates formed from linear polyelectrolytes (PEs) and oppositely charged spherical colloids, such as globular proteins, solid nanoparticles, or spherical micelles of ionic surfactants. At low concentrations, in stoichiometric solutions, PEs adsorb at the colloids to form electrically neutral finite-size complexes. These clusters attract each other through bridging between the adsorbed PE layers. Above a threshold concentration, macroscopic phase separation sets in. The coacervate internal structure is defined by (i) the adsorption strength and (ii) the ratio of the resulting shell thickness to the colloid radius, H/R. A scaling diagram of different coacervate regimes is constructed in terms of the colloid charge and its radius for Θ and athermal solvents. For high charges of the colloids, the shell is thick, $H \gg R$, and most of the volume of the coacervate is occupied by PEs, which determine its osmotic and rheological properties. The average density of hybrid coacervates exceeds that of their PE–PE counterparts and increases with nanoparticle charge, Q. At the same time, their osmotic moduli remain equal, and the surface tension of hybrid coacervates is lower, which is a consequence of the shell's inhomogeneous density decreasing with the distance from the colloid surface. When charge correlations are weak, hybrid coacervates remain liquid and follow Rouse/reptation dynamics with a Q-dependent viscosity, $\eta_{Rouse} \sim Q^{4/5}$ and $\eta_{rep} \sim Q^{28/15}$ for a Θ solvent. For an athermal solvent, these exponents are equal to 0.89 and 2.68, respectively. The diffusion coefficients of colloids are predicted to be strongly decreasing functions of their radius and charge. Our results on how Q affects the threshold coacervation concentration and colloidal dynamics in condensed phases are consistent with experimental observations for *in vitro* and *in vivo* studies of coacervation between supercationic green fluorescent proteins (GFPs) and RNA.

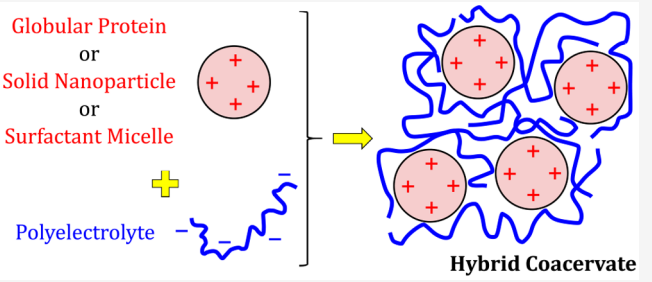

1. INTRODUCTION

Conventional polyelectrolyte complex coacervates, also known as interpolyelectrolyte complexes, are formed from oppositely charged polyelectrolytes (PEs), which adopt extended conformations in the absence of their complexation partners. In recent years, much progress has been made toward developing a comprehensive understanding of the equilibrium structure and dynamics of conventional coacervates. Experiments have revealed how the properties of the PEs, including their hydrophobicity, pH sensitivity, stereochemistry, stiffness, or fraction and sequence of ionic and neutral monomers influence their coacervation. Similarly, our theoretical understanding of conventional coacervates has advanced considerably, and it is now possible to predict their structural and thermodynamic properties with confidence.[1,2]

In contrast, much less is known about the electrostatically driven phase separation of solutions of PEs and other oppositely charged entities, such as solid colloidal particles, micelles of ionic surfactants, or globular proteins. In what follows, we refer to the resulting macroscopic condensed phases as "hybrid coacervates", to reflect their similarity with conventional PE coacervates while recognizing key compositional differences between them. By introducing new constituents into coacervates, it becomes possible to modify their physical properties and endow them with new functionalities. For instance, globular proteins may provide enzymatic activity, thereby making the resulting hybrid coacervates not only structurally but also catalytically reminiscent of membraneless organelles.

Dubin and co-workers were among the first to study hybrid coacervation between oppositely charged globular proteins and polysaccharides/linear synthetic PEs.[3] Their comprehensive reviews, refs 4 and 5, provide a summary of early activity in this area. These authors found that the formation of the hybrid coacervate phase is sensitive to the pH, which affects the net

Received: December 6, 2022
Revised: January 28, 2023
Published: February 14, 2023

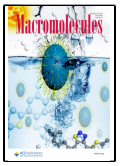

charge of the constituents, particularly proteins.[5,6] Klemmer et al. reported that the optimal pH value for coacervation, which was quantified from solution turbidity measurements, corresponds to charge stoichiometric conditions, leading to the formation of charge-balanced coacervates.[7] The phase separation in polysaccharide-protein systems was shown to consist of either complex coacervation or precipitation of solids.[6] The former represents a thermodynamic equilibrium state, and leads to a liquid−liquid phase coexistence, while the latter is irreversible and kinetically controlled. Increasing the ionic strength of the solution favors complex coacervation as opposed to the solid complex formation,[6] just as in the case of conventional coacervation of linear PEs.[8]

Recent advances in protein-based coacervation are discussed in ref 9 and support the earlier findings. Cummings and Obermeyer studied the complexation between variants of globular green fluorescent protein (GFP) and oppositely charged polyanions. Distinct GFP variants carried net charges ranging between $Q/e = +2$ and $Q/e = +26$. It was observed that increasing GFP charge promotes coacervation over a wider range of salt concentrations and pH.[10] Furthermore, this tendency, first detected *in vitro*, holds *in vivo*. Supercationic GFP was shown to trigger the formation of intracellular condensates with anionic RNA in *E. coli*, provided that the GFP total charge was sufficiently high.[11]

Subsequent work from the same group demonstrated that, in addition to the net protein charge, Q, the blockiness of the charge distribution also influences the phase behavior of protein−PE solutions.[12] Proteins with higher charge "patchiness" were found to form hybrid coacervates with higher salt resistance. Similar results were reported for other mutants of GFP, and a parameter that measures the charge patchiness was introduced to quantify the distribution of the ionic monomers on the surface of the GFP globule.[13]

The results of refs 9−13 illustrate the similarity between hybrid and conventional coacervates. In the latter, increasing the total charge of PEs for a fixed length (i.e., without changing the translational entropy) is achieved by incorporating a higher fraction of ionic monomers, which, in a similar way, leads to enhanced coacervate stability against salt.[14,15] The more subtle role of charge blockiness in conventional interpolyelectrolyte coacervation is analogous, albeit other determinants are required to define the 1D blockiness in the linear (primary) sequence of PE monomers[16,17] as compared to the 2D interfacial charge patchiness encountered in globular proteins.

Theoretical treatments of hybrid complex coacervation between linear flexible PEs and oppositely charged spherical nanoparticles—globular proteins, micelles of ionic surfactants, or solid colloids—have been limited, and analytical approaches are not available in the literature. Ganesan et al. combined the single chain in mean-field methodology with Monte Carlo simulations to examine the role of charge patchiness on hybrid coacervation, particularly the adsorption of PEs on spherical nanoparticles and the aggregation induced by PE bridging.[18−20] Madinya and Sing used a hybrid Monte Carlo and self-consistent field theory model to consider hybrid coacervates formed from PEs and worm-like surfactant micelles, but that approach has not been extended to spherical micelles.[21] The aforementioned numerical frameworks have only considered the equilibrium properties of hybrid coacervates, and discussions of their dynamics or rheology are not available.

In this work, a scaling approach is employed to fill the existing gap in our theoretical understanding of hybrid coacervates, and we use it to arrive at analytical predictions of both their structural and dynamical (rheological) properties. An important aspect of our scaling theory is that it serves to establish a connection with the closely related phenomena of (i) conventional polyelectrolyte complex coacervation[22−24] and (ii) the adsorption of PEs at oppositely charged interfaces,[25−28] both of which are well understood within the scaling framework. The latter enables performing a direct comparison between the properties of hybrid coacervates and that of their conventional counterparts.

We adopt a minimal theoretical model of a hybrid coacervate in which the colloid is represented by an impenetrable sphere of radius R carrying charge Q. We assume that the charge is uniformly distributed on the nanoparticle surface. The effect of the interfacial charge patchiness is more demanding and will be considered in future work. PEs are modeled as flexible Gaussian chains of length N carrying a fraction f of ionic monomers.

The article is organized as follows. In Section 2, we consider electroneutral pairs formed from one colloid particle and one PE chain of equal charge, $Q = fN$. This electroneutral colloid−PE complex represents the elementary cell of a hybrid coacervate for any $Q \neq fN$. The internal structure of the PE layer adsorbed at the nanoparticle depends on the problem parameters, and several scaling regimes are delineated. In Section 3, by calculating the free energy of the PE adsorption, we determine the thermodynamic regime for the formation of the colloid−PE pair. Attractions between neutral pairs are provided by bridging interactions, and their free energy is calculated in Section 4 in order to predict the range of macroscopic hybrid coacervation. These results are summarized in a scaling diagram that shows the regions of adsorption and hybrid coacervation. Section 5 provides the critical association concentrations between single colloids and PEs and threshold concentrations for macroscopic phase separation. The generalization of our results to neutral but charge-unmatched complexes, where one PE chain neutralizes several nanoparticles, $Q = iN$ with $i > 1$, is provided in Section 6. The osmotic and rheological properties of hybrid coacervates of arbitrary $Q < fN$ are considered in Sections 7 and 8, respectively. Section 9 summarizes our findings about hybrid coacervate structure and dynamics and discusses them in the context of available experimental data.

2. ADSORPTION OF A POLYELECTROLYTE ON A COLLOIDAL PARTICLE: STRUCTURE OF A SINGLE COLLOID−POLYELECTROLYTE PAIR

We consider a stoichiometric solution of oppositely charged, charged-matched colloidal particles and PEs. Each flexible PE consists of N monomers, with a fraction f of charged monomers, and carries a charge fN (expressed in e units). The dimensionless Bjerrum length is denoted by u; $u = e^2/\epsilon b k_B T$, where b is the size of the monomer. The absolute charge of the spherical nanoparticle Q is equal to that of the PE, $Q = fN$. (In fact, the results of this section are valid for any $Q > fN$, as discussed later in Section 4.) The nanoparticle radius is denoted by R. In what follows, all lengths are given in b units, all charges in e units, and all energies in units of $k_B T$. We consider colloids much larger than the monomer, $R \gg 1$, when the ion pairing effect is negligible. Due to the charge match between colloids and PEs, their concentrations (number densities) in solution are equal and denoted by c. We limit our analysis to Θ solvent conditions, with the dimensionless third virial $w \simeq 1$. For simplicity, we consider a counterion-free and salt-free solution.

We begin by examining the adsorption of a single PE at a colloid. Building on the available results for flat surface

https://doi.org/10.1021/acs.macromol.2c02464
Macromolecules 2023, 56, 1713−1730

adsorption,[25,27−29] we distinguish the regimes of weak and strong adsorption. In the weak adsorption regime, the thickness of the layer H is defined by the balance between Coulomb colloid−PE attractions and the conformational entropy of the compressed PE.[25] In the strong adsorption regime, the layer structure is controlled by the interplay between Coulomb attractions and short-range (three-body) repulsions between the monomers of the PE.[28] The geometry of the problem requires that the cases (scaling regimes) of quasi-planar and essentially spherical adsorption also be distinguished, with $H \ll R$ and $H \gg R$, respectively.

2.1. Strong Spherical Adsorption (Regime I). A neutral colloid−PE pair can be considered as the positively charged sphere of radius R, which is surrounded by a homogeneously and oppositely charged PE layer of the thickness H. The Coulomb energy of this configuration of charges (expressed in k_BT units) can be estimated as

$$F_{Coul}^{I} \simeq uQ^2\left(\frac{1}{R} - \frac{1}{H}\right) \tag{1}$$

This result shows that, at the scaling level of accuracy, it can be considered the Coulomb energy of the spherical capacitor with the plates of radii R and $R + H \simeq H$. This is because the distribution of the negative charge−either its concentration on the outer sphere as in a real capacitor or its uniform distribution over the volume between the spheres as in the considered PE layer−affects only the omitted numerical prefactor and does not change the scaling estimate for the electrostatic energy.

The volume of the adsorbed layer (capacitor) equals $V \simeq H^3$, and the free energy of three-body repulsions is given by

$$F_{vol}^{I} \simeq Vw\left(\frac{N}{V}\right)^3 \simeq \frac{Q^3}{f^3H^6} \tag{2}$$

where the charge-matching condition $fN = Q$ has been used. Here we have assumed that the PE shell of the nanoparticle is homogeneous. Taking into consideration the density inhomogeneity, which is discussed in Appendix A, does not change our estimates. Minimization of the total free energy $F_{Coul}^{I} + F_{vol}^{I}$ with respect to H yields

$$H_I \simeq u^{-1/5}f^{-3/5}Q^{1/5} \tag{3}$$

This result is consistent with the findings of ref 23 for a PE complex coacervate of short polycations with a high linear charge density and long polyanions with a low linear charge density (see eq 32 therein). The average density of the polymer within the adsorbed layer is equal to

$$\phi_I \simeq \frac{N}{H^3} \simeq \frac{Q}{fH^3} \simeq u^{3/5}f^{4/5}Q^{2/5} \tag{4}$$

The free energy of short-range repulsions can be calculated from eqs 2 and 3 and (the absolute value) reads:

$$F_{vol}^{I} \simeq \frac{uQ^2}{H_I} \simeq u^{6/5}f^{3/5}Q^{9/5} \tag{5}$$

The boundary between the spherical and quasi-planar regimes of strong adsorption, I and II, can be found from the equality $H_I \simeq R$:

$$Q_{I/II} \simeq uf^3R^5 \tag{6}$$

and spherical regime I is implemented at $Q \gg Q_{I/II}$.

To determine the boundary with the regime of weak spherical adsorption, IV, one can calculate the conformational energy of PEs confined within a layer of thickness H

$$F_{conf}^{I} \simeq \frac{N}{H_I^2} \simeq u^{2/5}f^{1/5}Q^{3/5} \tag{7}$$

and compare it to the energy of short-range repulsions, eq 5. In regime I, short-range interactions dominate over the conformational entropy, $F_{vol}^{I} \gg F_{conf}^{I}$. This requirement is fulfilled for $Q \gg Q_{I/IV}$ with

$$Q_{I/IV} \simeq q_e \simeq u^{-2/3}f^{-1/3} \tag{8}$$

Here q_e is the charge of the electrostatic blob in a Θ solvent. To provide $q_e \gg 1$, we assume that the condition

$$uf^{1/2} \ll 1 \tag{9}$$

is fulfilled in the following considerations.

The free energy of PE adsorption can be calculated as the change in the energy of the electric field due to colloid−PE pairing, $F_{ads}^{I} \simeq F_{Coul}^{I} - F_{Coul}^{np} - F_{Coul}^{PE}$. A free PE can be viewed as a stretched sequence of electrostatic blobs,[29,30] and the PE self-energy is equal to the number of blobs in the chain

$$F_{Coul}^{PE} \simeq \frac{N}{g_e} \simeq u^{2/3}f^{4/3}N \simeq u^{2/3}f^{1/3}Q \tag{10}$$

The energy of the field near a nonpaired nanoparticle is given by

$$F_{Coul}^{np} \simeq u\frac{Q^2}{R} \tag{11}$$

It decreases as a result of pairing, and in the paired state F_{Coul}^{I} is given by eq 1. It is seen that the adsorption energy is equal to the change in the electric field energy around the nanoparticle

$$F_{ads}^{I} \simeq -\frac{uQ^2}{H_I} \simeq -u^{6/5}f^{3/5}Q^{9/5} \tag{12}$$

because this change dominates the self-energy of the PE, $F_{Coul}^{PE}/F_{ads}^{I} \simeq (q_e/Q)^{4/5} \ll 1$. (The latter follows from the higher number of blobs in the PE shell as compared to the free PE.) We note that the equality between the absolute values of F_{ads}^{I} and F_{vol}^{I} is due to the spherical geometry of the adsorbed layer and does not hold when the adsorbed layer becomes quasi-planar, as will be demonstrated in the following subsection.

2.2. Strong Quasi-planar Adsorption (Regime II). In the quasi-planar regime II, the Coulomb energy of the adsorbed layer (capacitor) reads

$$F_{Coul}^{II} \simeq uQ^2\left(\frac{1}{R} - \frac{1}{R+H}\right) \simeq uQ^2\frac{H}{R^2} \tag{13}$$

owing to $H \ll R$. The layer (capacitor) volume is equal to R^2H, and the energy of three-body repulsions can be estimated as

$$F_{vol}^{II} \simeq Vw\left(\frac{N}{V}\right)^3 \simeq \frac{Q^3}{f^3H^2R^4} \tag{14}$$

The balance between F_{Coul}^{II} and F_{vol}^{II} controls the equilibrium thickness of the adsorbed layer

$$H_{II} \simeq u^{-1/3}f^{-1}\sigma^{1/3} \simeq u^{-1/3}f^{-1}\left(\frac{Q}{R^2}\right)^{1/3} \tag{15}$$

https://doi.org/10.1021/acs.macromol.2c02464
Macromolecules 2023, 56, 1713−1730

This result coincides with that reported for the adsorption at a planar interface.[27,28] Remarkably, in the quasi-planar case, the dependence of the thickness H on Q and R can be reduced to the dependence on the combination $\sigma = Q/R^2$ that expresses the surface charge density of the ball. This result is expected for any regime of quasi-planar adsorption. The average polymer density within the PE shell of the nanoparticle is given by

$$\phi_{II} \simeq \frac{N}{R^2 H} \simeq u^{1/3}\sigma^{2/3} \simeq u^{1/3}\left(\frac{Q}{R^2}\right)^{2/3} \tag{16}$$

The energy of three-body volume interactions per one colloid−PE pair equals

$$F_{vol}^{II} \simeq u^{2/3} f^{-1} Q^{7/3} R^{-8/3} \tag{17}$$

The requirement of the thin adsorbed layer, $H_{II} \ll R$, yields $Q \ll Q_{I/II}$ with the crossover value $Q_{I/II}$ defined by eq 6. Planar adsorption remains strong until the conformational free energy of the PE

$$F_{conf}^{II} \simeq \frac{N}{H^2} \simeq u^{2/3} f Q^{1/3} R^{4/3} \tag{18}$$

is much lower than the free energy of three-body repulsions, $F_{vol}^{II} \simeq F_{ads}^{II}$. Therefore, one arrives at the condition $Q \gg Q_{II/III}$ with

$$Q_{II/III} \simeq fR^2 \tag{19}$$

This crossover between the planar regimes of strong and weak adsorption, II and III, can be also written as $\sigma_{II/III} \simeq f$, or equivalently, $\sigma_{II/III} \simeq \sigma_e$ with $\sigma_e \simeq q_e/\xi_e^2 = f$ being the surface charge density of the electrostatic blob.[27,28]

The adsorption energy can be calculated as $F_{ads}^{II} = F_{Coul}^{II} - F_{Coul}^{np} - F_{Coul}^{PE}$. In the regime of planar adsorption, the term corresponding to the nanoparticle self-energy dominates because $F_{Coul}^{II}/F_{Coul}^{np} \simeq H_{II}/R \ll 1$ and $F_{Coul}^{PE}/F_{Coul}^{np} \simeq \xi_e\sigma_e/R\sigma \ll 1$. The final result

$$F_{ads}^{II} \simeq -F_{Coul}^{np} \simeq -u\frac{Q^2}{R} \tag{20}$$

shows that the electric field around the nanoparticle is almost entirely neutralized by the PE owing to the small thickness of the adsorbed layer, $H_{II} \ll R$.

2.3. Weak Quasi-planar Adsorption (Regime III). The balance between the layer (capacitor) Coulomb energy, $F_{Coul}^{III} \simeq uQ^2H/R^2$, and the conformational entropy of the PE, $F_{conf}^{III} \simeq Q/fH^2$, defines the layer thickness

$$H_{III} \simeq (uf\sigma)^{-1/3} \simeq \left(uf\frac{Q}{R^2}\right)^{-1/3} \tag{21}$$

This result has been reported earlier; see refs 25, 27, and 28. The average density of the adsorbed layer reads

$$\phi_{III} \simeq \frac{N}{R^2 H} \simeq u^{1/3} f^{-2/3} \sigma^{4/3} \simeq u^{1/3} f^{-2/3}\left(\frac{Q}{R^2}\right)^{4/3} \tag{22}$$

and the Coulomb energy of the layer is on the order of

$$F_{Coul}^{III} \simeq u^{2/3} f^{-1/3} Q^{5/3} R^{-4/3} \tag{23}$$

The boundary II/III between weak and strong adsorption is given by eq 19. The crossover III/IV between the quasi-planar and spherical cases, $H_{III} \simeq R$, can be written as

$$Q_{III/IV} \simeq (ufR)^{-1} \tag{24}$$

with regime III arising at $Q \gg Q_{III/IV}$.

The adsorption energy can be found from $F_{ads}^{III} = F_{Coul}^{III} - F_{Coul}^{np}$. Here we do not subtract the self-energy of the PE because the adsorption is weak, and the blob structure of the polycation remains unchanged,[25] as discussed later in Section 4.3. Similar to regime II, $F_{Coul}^{III}/F_{Coul}^{np} \simeq H_{III}/R \ll 1$ and the adsorption energy in the quasi-planar regime III is of the order of the energy of the electric field near a bare nanoparticle:

$$F_{ads}^{III} \simeq -u\frac{Q^2}{R} \tag{25}$$

2.4. Weak Spherical Adsorption (Regime IV). In the next section, we explain why this adsorption regime is in fact absent; the adsorption energy is extremely low and never exceeds the thermal energy k_BT. We begin with a standard analysis. The equality between the Coulomb energy of colloid−PE attractions, $F_{Coul}^{IV} \simeq uQ^2/R - uQ^2/H$, and the conformational free energy of the PE, $F_{conf}^{IV} \simeq Q/fH^2$, results in

$$H_{IV} \simeq (ufQ)^{-1} \tag{26}$$

The average layer density equals

$$\phi_{IV} \simeq \frac{N}{H^3} \simeq u^3 f^2 Q^4 \tag{27}$$

The adsorption energy is defined by the energy of the electric field in the vicinity of the colloid

$$F_{ads}^{IV} \simeq -u\frac{Q^2}{H_{IV}} \simeq -u^2 f Q^3 \tag{28}$$

because the local blob structure of the PE remains unchanged upon adsorption.

The crossover I/IV between the weakly and strongly adsorbed spherical layers is defined by eq 8. The boundary III/IV between the weak spherical and weak planar regimes can be found from $H_{IV} \simeq R$ and leads to eq 24.

Here we note that, in all scaling regimes, we do not expect a complexation-induced charge-reversal of the colloid because the solutions considered here are stoichiometric and the colloid−PE pair is charge-matched. Charge reversal may be expected for charge-unmatched systems with $Q \neq fN$.[31−35] Additionally, the final purpose of our analysis is to describe the structure and properties of the macroscopic hybrid coacervate phases, which are globally neutral. We assume that single colloid−PE pairs are the elementary electroneutral cells of the resulting macroscopic assemblies.

3. ADSORPTION BOUNDARIES

All possible adsorption regimes have now been delineated, and the boundaries between them are known. Remarkably, all crossover lines (I/II, II/III, III/IV, and I/IV) intersect at the same point with the coordinates

$$R \simeq \xi_e \simeq (uf^2)^{-1/3} \tag{29}$$

$$Q \simeq q_e \simeq u^{-2/3} f^{-1/3} \tag{30}$$

where ξ_e is the size of the electrostatic blob in a Θ solvent. The boundaries between the regimes of adsorption (colloid−PE paring) can be therefore written as

$$Q_{I/II} \simeq q_e\left(\frac{R}{\xi_e}\right)^5 \tag{31}$$

https://doi.org/10.1021/acs.macromol.2c02464
Macromolecules 2023, 56, 1713−1730

$$Q_{II/III} \simeq q_e\left(\frac{R}{\xi_e}\right)^2 \tag{32}$$

$$Q_{III/IV} \simeq q_e\left(\frac{R}{\xi_e}\right)^{-1} \tag{33}$$

$$Q_{I/IV} \simeq q_e \tag{34}$$

To determine whether adsorption (i.e., the formation of neutral colloid−PE pairs) takes place, the adsorption energies can be expressed as follows

$$|F_{ads}^{I}| \simeq \left(\frac{Q}{q_e}\right)^{9/5} \gg 1 \tag{35}$$

$$|F_{ads}^{II}| \simeq \left(\frac{Q}{q_e}\right)^{2}\frac{\xi_e}{R} \gg 1 \tag{36}$$

$$|F_{ads}^{III}| \simeq \left(\frac{Q}{q_e}\right)^{2}\frac{\xi_e}{R} \tag{37}$$

$$|F_{ads}^{IV}| \simeq \left(\frac{Q}{q_e}\right)^{3} \ll 1 \tag{38}$$

and their values can be compared with thermal energy. In regimes I and II, the adsorption always occurs, while in regime IV it never takes place. For regime III, the adsorption happens only for $|F_{ads}^{III}| \gg 1$, i.e., the adsorption threshold (within regime III, for $R \gg \xi_e$) reads $Q \gg Q_{ads}$ with

$$Q_{ads} \simeq q_e\left(\frac{R}{\xi_e}\right)^{1/2} \tag{39}$$

The resulting adsorption diagram, i.e., the diagram of the pairing between colloids and PEs, is shown in Figure 1. On this diagram, all logarithmic terms, which appear from the decrease of the translational entropy of adsorbed PEs as compared to the free unbound PEs, are neglected.

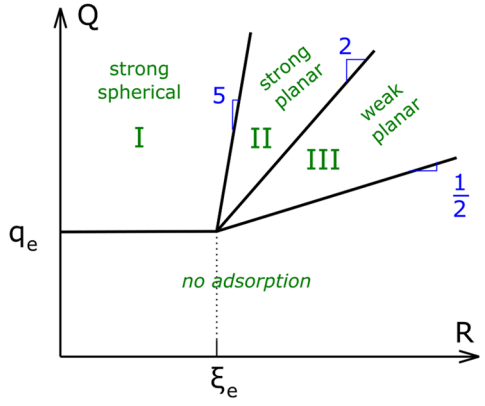

Figure 1. Diagram showing the various adsorption regimes. The boundary $Q_{III/IV} \sim R^{-1}$ is not explicitly shown as it lies within the region of no adsorption and has no physical meaning.

4. BRIDGING INTERACTIONS AND MACROSCOPIC COACERVATION

To find the conditions under which macroscopic coacervation takes place, one must calculate the free energy gain due to the formation of the macroscopic coacervate phase from single electroneutral colloid−PE pairs. This gain is provided by bridging interactions, which have an entropic nature[36−39] and are schematically shown in Figure 2. Briefly, when two adsorbed layers are in contact, each PE chain reaching the middle plane between the neighboring colloids can either fold back and form a loop or cross this plane and form a bridge. If colloids are separated, bridging is impossible and all the chains must form loops, which diminishes the conformational entropy of PE by k_BT per bridge/loop. Therefore, the entropic gain due to bridging is of order the number of blobs in the middle plane. It should be noted that zero charge of colloid−PE pairs makes bridging between them analogous to that in nonionic polymers; this enables following the lines of the respective neutral polymers literature, refs 36−39.

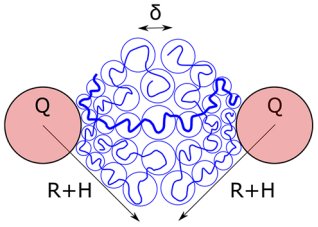

Figure 2. Schematic illustration of bridging interactions between neutral colloid−PE pairs. The bridging chain is shown with a thick line.

4.1. Strong Spherical Adsorption (Regime I). The inhomogeneous structure of the adsorbed layer in regime I is discussed in Appendix A and shown in Figure A1. A detailed analysis shows that the polymer density is higher in the vicinity of the ball, and lower at the shell periphery, due to the partial screening of the ball charge by the PEs. The size of the average blob within the PE shell is lower than that of the outmost blob. The latter is equal to the electrostatic blob size, $\xi_{out} \simeq \xi_e$. The depth of the interpenetration between the polymer shells of two neutral colloid−PE pairs is on the order of the outmost blob size:[38,39]

$$\delta_I \simeq \xi_{out} \simeq \xi_e \simeq (uf^2)^{-1/3} \tag{40}$$

Simple geometric considerations show that, in regime I, the area of the interpenetration of the shells reads $A_I \simeq \delta_I H_I \simeq \xi_e H_I$ owing to $H_I \gg R$.[36,38,39] The free energy gain due to bridging can be estimated by k_BT per blob:

$$F_{br}^{I} \simeq -\frac{A_I}{\xi_e^{\,2}} \simeq -\frac{H_I}{\xi_e} \simeq -u^{2/15}f^{1/15}Q^{1/5} \simeq -\left(\frac{Q}{q_e}\right)^{1/5} \tag{41}$$

This is due to the number of neighbors that a pair has, i.e., the colloidal coordination number, which is on the order of unity. In Section 7, the results of eqs 40 and 41 will be derived more rigorously. One can see that $|F_{br}| \gg 1$ in regime I, leading to the formation of the macroscopic coacervate. If the logarithmic (concentration) corrections are omitted, the boundary $Q \simeq q_e$ serves as the crossover for both colloid−PE pairing and macroscopic coacervation.

https://doi.org/10.1021/acs.macromol.2c02464
Macromolecules 2023, 56, 1713−1730

The excess surface energy of the hybrid coacervate arises because PEs at the coacervate−supernatant interface cannot form bridges, or at least form a much lower number of them as compared to the chains in the phase bulk. According to the definition, the surface tension can be calculated as the ratio between the excess free energy, which is equal to the minus free energy of bridging, to the interfacial area occupied by one colloid−PE pair. The surface tension of the colloid−PE coacervate in regime I therefore equals

$$\gamma_I \simeq \frac{|F_{br}^I|}{H_I^2} \simeq \frac{1}{\xi_e H_I} \simeq u^{8/15} f^{19/15} Q^{-1/5} \simeq \gamma_e \left(\frac{q_e}{Q}\right)^{1/5} \tag{42}$$

Here $\gamma_e \simeq \xi_e^{-2}$ is the surface tension of the corresponding charge-density-symmetric PE−PE coacervate.[22,23,44] The surface tension of the colloid−PE coacervate is much lower, $\gamma_I \ll \gamma_e$.

4.2. Strong Quasi-planar Adsorption (Regime II). For regime II, the structure of the adsorbed layer and the size of the outmost blob, $\xi_{out} \simeq \xi_e$, have been presented in ref 28 and are rederived in Appendix A. The interpenetration depth reads $\delta_{II} \simeq \xi_e$, and the area of the shells' contact equals $A_{II} \simeq \delta_{II} R \simeq \xi_e R$ owing to $R \gg H_{II}$.[36] This leads to the free energy of bridging interactions given by

$$F_{br}^{II} \simeq -\frac{A_{II}}{\xi_e^2} \simeq -\frac{R}{\xi_e} \simeq -(uf^2)^{1/3} R \tag{43}$$

Due to $R \gg \xi_e$ in regime II, $F_{br}^{II} \gg 1$ and macroscopic complex coacervation is ensured. Similar to regime I, the surface tension of the coacervate in regime II

$$\gamma_{II} \simeq \frac{|F_{br}^{II}|}{R^2} \simeq \frac{1}{\xi_e R} \simeq (uf^2)^{1/3} R^{-1} \simeq \gamma_e \frac{\xi_e}{R} \tag{44}$$

is low compared to that of its symmetric PE−PE counterpart, $\gamma_{II} \ll \gamma_e$.

At the crossover II/III, the interpenetration depth of the adsorbed layers is of the order of the total layer height, $H_{II} \simeq \xi_e \simeq \delta_{II}$. The colloid−PE pair can be viewed as a colloid covered by a continuous but narrow layer of electrostatic blobs. At that, only ξ_e/R fraction of these blobs simultaneously serves as the bridges.

4.3. Weak Quasi-planar Adsorption (Regime III). In regime III, the adsorbed layer becomes even more sparse and fuzzy, leading to $\delta_{III} \simeq H_{III}$, as shown in Figure 3. Therefore, the contact area equals $A_{III} \simeq R\delta_{III} \simeq RH_{III}$.

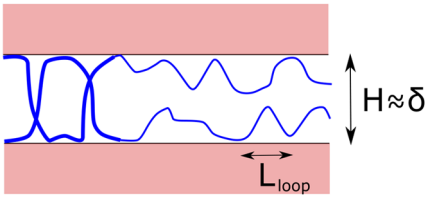

Figure 3. Schematic illustration of bridging interactions between flat adsorbed layers, $R \gg H$. The Bridging fragment of the PE is shown with a thick line.

To estimate the free energy gain due to bridging, we find the size of one loop (the number of monomers in it, n_{loop}) and the average colloid area per one loop. In regime III, Coulomb attractions between the colloids and the PEs are balanced by the entropy of PE compression.[25] In the direction *perpendicular to the surface*, PE loops exhibit ideal random walk statistics, and the number of monomers per one loop can be estimated as follows:

$$n_{loop} \simeq H_{III}^2 \simeq (uf\sigma)^{-2/3} \tag{45}$$

The total number of loops surrounding one ball is much higher than unity, $N/n_{loop} \simeq (Q/q_e)^{5/3}(\xi_e/R)^{4/3} \gg 1$. This allows us to neglect the presence of tails (1 per ball), which may generate repulsive interactions.[45] The average colloid area per one loop can be found from the charge balance condition:

$$S_{loop} \simeq \frac{n_{loop} f}{\sigma} \simeq u^{-2/3} f^{1/3} \sigma^{-5/3} \tag{46}$$

One can also obtain this result using $S_{loop} \simeq R^2 n_{loop}/N$. It is worth noting that S_{loop} is *not* equal to the squared lateral length of the loop L_{loop}^2, with $L_{loop} \simeq \xi_e n_{loop}/g_e \simeq u^{-1/3}\sigma^{-2/3}$, because the loops do not densely cover the entire ball surface. The energy gain due to bridging is given by

$$F_{br}^{III} \simeq -\frac{A_{III}}{S_{loop}} \simeq -u^{1/3} f^{-2/3} Q^{4/3} R^{-5/3} \simeq -\left(\frac{Q}{q_e}\right)^{4/3} \left(\frac{\xi_e}{R}\right)^{5/3} \tag{47}$$

The formation of the macroscopic phase occurs when $|F_{br}^{III}| \gg 1$, i.e., when $Q \gg Q_{coac}$, with the corresponding crossover value

$$Q_{coac} \simeq u^{-1/4} f^{1/2} R^{5/4} \simeq q_e \left(\frac{R}{\xi_e}\right)^{5/4} \tag{48}$$

We emphasize that the thresholds for adsorption and coacervation in regime III are different:

$$\frac{Q_{coac}}{Q_{ads}} \simeq \left(\frac{R}{\xi_e}\right)^{3/4} \gg 1 \tag{49}$$

In other words, for $Q_{ads} \ll Q \ll Q_{coac}$, colloids and PEs do form neutral pairs, which in turn do not form a macroscopic phase and remain dispersed in the solution.

In regime III, for $Q \gg Q_{coac}$, the coacervate surface tension can be calculated in a standard manner:

$$\gamma_{III} \simeq \frac{|F_{br}^{III}|}{R^2} \simeq u^{1/3} f^{-2/3} Q^{4/3} R^{-11/3} \simeq \gamma_e \left(\frac{Q}{q_e}\right)^{4/3} \left(\frac{\xi_e}{R}\right)^{11/3} \tag{50}$$

4.4. Scaling Diagram of Hybrid Coacervation. Figure 4 summarizes the states of a colloid−PE solution. In Appendix B, we demonstrate that the appearance of this diagram remains qualitatively unchanged if a Θ solvent is substituted by an athermal solvent. In this diagram, we do not show the intermediate, logarithmically wide transition region between regimes I−III and the region of "absent adsorption". This level of accuracy is standard for a scaling analysis. In this intermediate region, one can expect adsorption but no coacervation. In contrast to the "only adsorption" regime with $Q_{ads} \ll Q \ll Q_{coac}$, this intermediate region has zero width if the logarithmic, concentration-dependent terms are neglected.

The diagram presented in Figure 4 allows one to predict how the coacervate properties will change as a function of the nanoparticles' size and charge. The respective dependencies are shown in Figures 5 and 6. Interestingly, in the quasi-planar regimes II and III, the shell thickness changes in a non-monotonic fashion as Q or R increases. For instance, shell thickness first decreases and then increases as the ball charge grows, $H_{III} \sim Q^{-1/3}$ in regime III and $H_{II} \sim Q^{1/3}$ in regime II. This

https://doi.org/10.1021/acs.macromol.2c02464
Macromolecules 2023, 56, 1713−1730

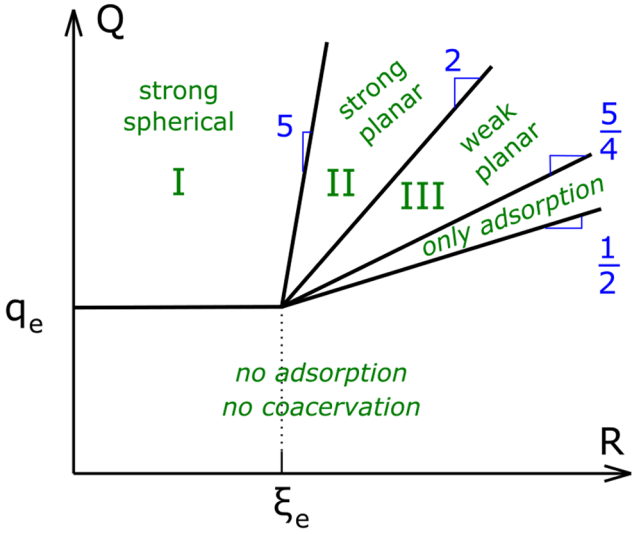

Figure 4. Diagram showing the various solution regimes. We distinguish (i) three different scaling regimes of complex coacervation, I–III; (ii) the "only adsorption" region, $Q_{ads} \ll Q \ll Q_{coac}$ and $R \gg \xi_e$, where coacervation is absent but PEs adsorb on the colloids; (iii) the region where both coacervation and adsorption are absent.

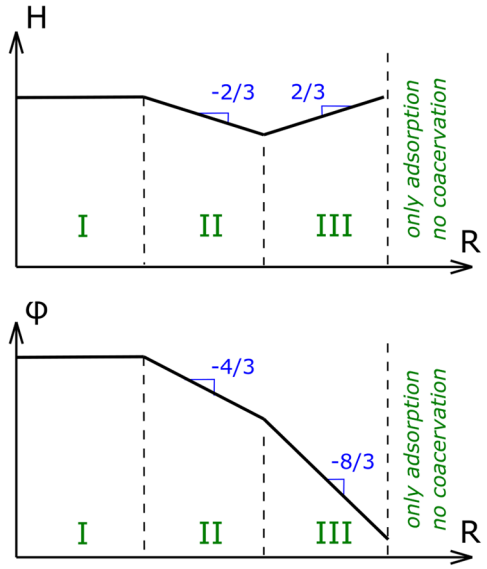

Figure 5. Dependence of the corona thickness, H, and polymer volume fraction, ϕ, on nanoparticle size, R.

behavior is the result of the two opposite tendencies. Increasing the particle's charge requires more PE to neutralize it, but simultaneously, the average shell density ϕ increases due to the increasing strength of Coulomb attractions. In regime III, the growth of the polymer density is strong, $\phi_{III} \sim Q^{4/3}$, which makes the second factor dominant and results in the decreasing shell thickness. In contrast, density increases slower than linearly in regime II, $\phi_{II} \sim Q^{2/3}$, which leads to the increasing thickness of the thin, quasi-planar shell, $H_{II} \sim Q^{1/3}$. An analogous behavior has been reported by Dobrynin et al. for the adsorption of PEs on a planar surface.[27,28]

4.5. Range of Applicability. *4.5.1. Counterion Condensation and Colloid Charge Regulation.* Our analysis is valid when PE adsorption is a more favorable mechanism for colloid neutralization than the condensation of small (univalent)

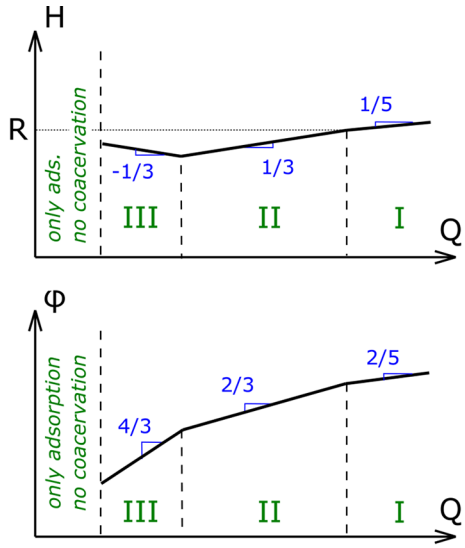

Figure 6. Dependence of the corona thickness, H, and polymer volume fraction, ϕ, on nanoparticle charge, Q.

counterions. The necessary requirements can be obtained by comparing the height of the counterion atmosphere near the colloid and the height of the adsorbed PE layer.

When the colloid charge is so small that the translational entropy of counterion exceeds the energy of Coulomb counterion-colloid interactions, $uQ/R \ll 1$, all counterions are almost homogeneously distributed in the solution.[46−48] One may argue that the concentration-dependent factor $\ln(1/cR^3)$ should be added to the right-hand side of the inequality,[48] but, within our treatment, we systematically neglect all logarithmic corrections. For a high charge of the colloid, $Q > Q_{ion}$ with $Q_{ion} \simeq R/u$, most counterions are trapped within the quasi-planar layer of a thickness equal to the Gouy−Chapman length, $l_{GC} \simeq 1/u\sigma \simeq R^2/uQ$.[48] We note that for $Q \gg Q_{ion}$ this thickness is much lower than the colloid radius, $l_{GC} \ll R$.

In regime I, the PE shell is thick, $H_I \gg R$, and the effect of counterion condensation, which results in the charge regulation of the colloid nanoparticle, is negligible only when $Q \ll Q_I^*$ with

$$Q_I^* \simeq Q_{ion} \simeq \frac{R}{u} \tag{51}$$

For regime II, of quasi-planar adsorption, a less stringent requirement $H_{II} \ll l_{GC}$ is sufficient. It can be written as $Q \ll Q_{II}^*$ with

$$Q_{II}^* \simeq u^{-1/2} f^{3/4} R^2 \tag{52}$$

or equivalently $\sigma \ll \sigma_{ion} \simeq u^{-1/2} f^{3/4}$. The latter result has been reported earlier for planar PE adsorption.[27,28] It provides a high number of ionic monomers within the blob most proximate to the PE shell, $f\xi_{prox}^2 \gg 1$, where ξ_{prox} is given by eq A7 of Appendix A. The cost for nanoparticle neutralization by PEs is due to short-range three-body repulsions between all PE monomers and is enthalpic, much lower than k_BT per charge. Neutralization of nanoparticle charge by counterions would lead to a diminution of their translational entropy, i.e., the free energy cost would be on the order of the thermal energy per charge. The latter is unfavorable until the most proximate blob contains only one ionic monomer.[28] In Section 8, we also assume that eq 52 is fulfilled in regime I to provide weak charge correlations even near the colloid interface.

https://doi.org/10.1021/acs.macromol.2c02464
Macromolecules 2023, 56, 1713−1730

In regime III, the necessary condition $H_{III} \ll l_{GC}$ is always fulfilled owing to eq 9.

To recapitulate, the scaling diagram shown in Figure 4 does not require modifications for systems without counterions, e.g. when they are washed out. In the presence of counterions, extra boundaries $Q \simeq Q_I^*$ and $Q \simeq Q_{II}^*$ should be added to limit Regimes I and II from the side of very high charges. Beyond these boundaries, condensation of small counterions sets in. This may result in the formation of nonstoichiometric hybrid coacervates, where the charge of colloids is neutralized partially by PEs and partially by counterions.[28] In this case, our predictions on the PE shell structure may remain a reasonable zeroth-order approximation, but the critical association concentrations are expected to change. We leave this problem for future work.

4.5.2. Effect of Salt. The considerations above were devoted to the salt-free case, $c_s = 0$, but the results presented thus far should also hold at sufficiently low c_s, until the point where salt perturbs the structure of the adsorbed PE layer. That occurs when the Debye length, $r_D \simeq u^{-1/2} c_s^{-1/2}$, is comparable to the length scale of Coulomb interactions in the system.[26,28] In regimes I and II, the latter is of the same order as the PE shell thickness, H. The equality $r_D \simeq H$ results in the following crossover concentrations between the scaling regimes of salt-free and salt-added adsorption:

$$c_s^{I,*} \simeq u^{-3/5} f^{6/5} Q^{-2/5} \tag{53}$$

$$c_s^{II,*} \simeq u^{-1/3} f^2 Q^{-2/3} R^{4/3} \tag{54}$$

The latter result has been earlier reported in ref 28 for the planar PE adsorption.

In regime III, the characteristic length of Coulomb interactions is defined by the lateral correlation length of the adsorbed PE layer, rather than its much lower thickness, $\xi_{lat} \gg H_{III}$. At lengths below ξ_{lat}, Coulomb repulsions between the monomers of a PE yield locally extended conformations, with the number of monomers per 2D mesh size equal to $g_{lat} \simeq g_e \xi_{lat}/\xi_e$. Using the colloid–PE charge balance written for the correlation area, $\sigma \xi_{lat}^2 \simeq f g_{lat}$, one can find $\xi_{lat} \simeq u^{-1/3} f^{1/3} \sigma^{-1}$.[28] Using $r_D \geq \xi_{lat}$, one can conclude that the salt-free results for regime III are applicable when the salt concentration is lower than

$$c_s^{III,*} \simeq u^{-1/3} f^{-2/3} Q^2 R^{-4} \tag{55}$$

4.5.3. On The Formation of Colloidal Crystal. The analysis above was limited to moderate-charge colloids when the hybrid coacervate phase is liquid/amorphous. If nanoparticles carry a very high charge and Coulomb coupling between them dominates polymer-mediated repulsions, formation of a colloidal crystal is expected. This crystal may be referred to as Wigner crystal owing to the electrostatically driven emergence of the colloidal long-range order. This problem requires separate consideration, which may be complicated by the need to calculate the exact numerical coefficients (unknown within the scaling approach) upon comparing the free energies of the disordered and different ordered states or applying the Lindemann criterion.

5. CRITICAL CONCENTRATIONS FOR ADSORPTION AND COACERVATION

The total concentration of colloids is equal to that of the PEs and is denoted by c. First, we consider the adsorption equilibrium and denote the concentration of free, nonpaired colloids/PEs c_{free}. The concentration of neutral colloid–PE pairs equals $c - c_{free}$. The equality between the free energies (chemical potentials) of the free and paired colloid–PE pair reads

$$2 \ln c_{free} = \ln(c - c_{free}) + \ln c_{conf} + F_{ads} \tag{56}$$

Here c_{conf} is the concentration of PEs in the confinement that takes into account the decrease of their translational entropy due to adsorption. For example, the volume available to the adsorbed PE in regime I is estimated as H_I^3, and $c_{conf}^I \simeq 1/H_I^3$. However, the exact calculation of c_{conf} only affects the pre-exponential factor in the final critical concentrations, while within our scaling analysis we have already omitted all numerical coefficients in the free energies, which define the exponent values. Assuming $c_{conf} \simeq 1$, the critical concentrations for adsorption can be found using $c_{free} \simeq c/2$:

$$c_{ads}^I \simeq e^{F_{ads}^I} \simeq \exp\left[-\left(\frac{Q}{q_e}\right)^{9/5}\right] \tag{57}$$

$$c_{ads}^{II} \simeq e^{F_{ads}^{II}} \simeq \exp\left[-\left(\frac{Q}{q_e}\right)^{2} \frac{\xi_e}{R}\right] \tag{58}$$

$$c_{ads}^{III} \simeq e^{F_{ads}^{III}} \simeq \exp\left[-\left(\frac{Q}{q_e}\right)^{2} \frac{\xi_e}{R}\right] \tag{59}$$

In a similar fashion, one can find the critical concentrations for coacervate formation. At $c \gg c_{ads}$, when almost all colloids and PEs are paired, their neutral pairs start forming bridges. We denote by c_{pair} the concentration of the neutral pairs. Coacervation arises from the free energy gain due to bridging, F_{br}, but simultaneously leads to the loss of translational entropy of the neutral pairs (balls):

$$\ln c_{pair} = \ln c_{ball} + F_{br} \tag{60}$$

Here c_{ball} is the concentration of neutral pairs (colloids) in the macroscopic coacervate phase. Again, to be consistent, we neglect the logarithmic term and assume $c_{ball} \simeq 1$. The threshold concentration for complex coacervation can be estimated from $c \simeq c_{pair}$ and corresponds to the situation when half of the colloids/PEs are involved in neutral pairs and half of them form the macroscopic coacervate phase:

$$c_{coac}^I \simeq e^{F_{br}^I} \simeq \exp\left[-\left(\frac{Q}{q_e}\right)^{1/5}\right] \tag{61}$$

$$c_{coac}^{II} \simeq e^{F_{br}^{II}} \simeq \exp\left[-\frac{R}{\xi_e}\right] \tag{62}$$

$$c_{coac}^{III} \simeq e^{F_{br}^{III}} \simeq \exp\left[-\left(\frac{Q}{q_e}\right)^{4/3} \left(\frac{\xi_e}{R}\right)^{5/3}\right] \tag{63}$$

The scaling diagram of states shown in Figure 4 is in accordance with the results for c_{ads} and c_{coac}. Similar to stoichiometric solutions of symmetric oppositely charged PEs,[40−43] the formation of electroneutral colloid–PE pairs takes place at much lower concentrations than macroscopic coacervation:

https://doi.org/10.1021/acs.macromol.2c02464
Macromolecules 2023, 56, 1713−1730

Table 1. Structural Properties of the Hybrid Coacervate in Regimes I–III: Scaling Laws for (i) the Thickness of the Adsorbed Layer, H; (ii) Average Polymer Density Within the PE shell, ϕ; (iii) Coacervate Surface Tension, γ

regime	adsorption type	H	ϕ	γ
I	strong spherical	$u^{-1/5}f^{-3/5}Q^{1/5}$	$u^{3/5}f^{4/5}Q^{2/5}$	$u^{8/15}f^{19/15}Q^{-1/5}$
II	strong quasi-planar	$u^{-1/3}f^{-1}Q^{1/3}R^{-2/3}$	$u^{1/3}Q^{2/3}R^{-4/3}$	$u^{1/3}f^{2/3}R^{-1}$
III	weak quasi-planar	$u^{-1/3}f^{-1/3}Q^{-1/3}R^{2/3}$	$u^{1/3}f^{-2/3}Q^{4/3}R^{-8/3}$	$u^{1/3}f^{-2/3}Q^{4/3}R^{-11/3}$

$c_{coac} \gg c_{ads}$ in all scaling regimes. This is due to the different strengths of the driving forces behind these processes. The bare Coulomb attractions that promote colloid–PE pairing and neutralization are much stronger than the entropic bridging interactions that generate the surface tension, which induces coalescence of the neutral pairs and, eventually, macroscopic coacervation.

In Appendix C, an alternative route to arrive at the same estimates for the threshold concentrations for coacervation is presented, which is based on the calculation of the second virial coefficient for the colloid–PE neutral pairs.[39]

6. GENERALIZATION TO COACERVATES WITH LONG POLYELECTROLYTES

In this section, we generalize our analysis to hybrid coacervates formed from colloid particles and PEs with unequal charges, $Q \neq fN$. We focus on the case when PEs are sufficiently long and their charge exceeds Q:

$$fN = iQ \tag{64}$$

For simplicity, we consider integer values of i, and $i = 1$ corresponds to the charge-matched systems considered above.

We emphasize that the equilibrium structure of the coacervates is independent of i, and the scaling laws summarized in Table 1 and Table B1 of Appendix B remain valid for any $Q \leq fN$. This is due to the minor role of the translational entropy of PEs within the macroscopic coacervate phase, which is negligible even for $N \simeq Q/f$. However, increasing i changes the structure of the elementary neutral aggregate, which should now comprise one PE and i nanoparticles that neutralize it. This renormalizes the energy of bridging interactions, and the coacervation boundary becomes i-dependent, as shown below.

First, we argue that the adsorption boundary, $Q \simeq Q_{ads}$, which is defined by the free energy gain of the colloid neutralization, remains unchanged and is given by eq 39. At the level of accuracy of our scaling analysis that neglects ln corrections, both the onset of the PE neutralization by colloids and the formation of the neutral complex of PE and i colloids take place at the same $Q \simeq Q_{ads}$.

However, the resulting neutral complex at the adsorption boundary does not have a spherical (globular) structure. One can consider the resulting complex as a quasi-polymer chain containing i quasi-monomers; each quasi-monomer consists of the colloidal particle and the surrounding shell, and its size is equal to $R + H \simeq R$. (Here we consider regime III as the closest to the "only adsorption" regime.) The structure of this quasi-polymer can be either linear or hyperbranched,[49] but, for simplicity, we limit our analysis to the first case. When bridging interactions are strong enough, the quasi-polymer aggregate undergoes a transition to globular conformations, and the radius of the resulting spherical globule is $R_{glob} \simeq i^{1/3}R$. In the globular state, the free energy gain due to the attractions of quasi-monomers, $F_{attr} \simeq -iF_{br}^{III}$, is proportional to the number of quasi-monomers i, and F_{br}^{III} is defined by eq 47. The conformational entropy loss of the quasi-polymer can be estimated as $F_{conf} \simeq iR^2/{R_{glob}}^2 \simeq i^{1/3}$. The collapse transition takes place when $F_{attr} \simeq F_{conf}$:

$${Q_{collpase}}^{i} \simeq i^{-1/2}Q_{coac} \simeq i^{-1/2}q_e\left(\frac{R}{\xi_e}\right)^{5/4} \tag{65}$$

The surface energy of the resulting globule is $\gamma \simeq F_{br}^{III}/R^2 \simeq \gamma_{III}$; see eq 50. The formation of the macroscopic coacervate phase takes place when the excess surface energy of the globule, $F_{surf} \simeq \gamma_{III}{R_{glob}}^2 \simeq i^{2/3}F_{br}^{III}$, is of the same order as the thermal energy. Up to the logarithmic concentration-dependent factors discussed in Section 5, the boundaries for the collapse of the quasi-polymer and for macroscopic coacervation coincide

$${Q_{coac}}^{i} \simeq {Q_{collpase}}^{i} \simeq i^{-1/2}Q_{coac} \simeq i^{-1/2}q_e\left(\frac{R}{\xi_e}\right)^{5/4} \tag{66}$$

The threshold value ${Q_{coac}}^{i}$ goes down with increasing i, and the region of the weak quasi-planar adsorption expands. This result slightly changes the morphology of the resulting scaling diagram

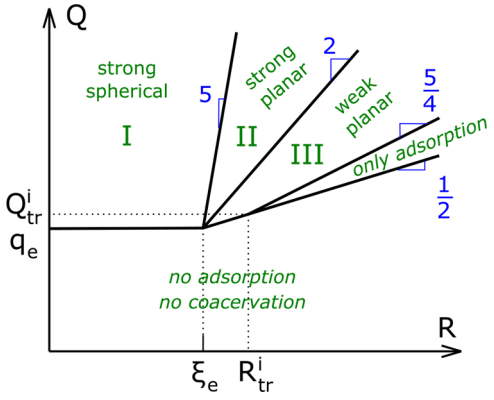

Figure 7. Diagram of the solution regimes for PEs and colloids with unequal charges, $fN/Q = i > 1$. The coordinates of the point $({R_{tr}}^{i}; {Q_{tr}}^{i})$ depend on i, and are given by eq 67.

of the solution, which is shown in Figure 7. The crossovers for adsorption and macroscopic coacervation intersect at

$${R_{tr}}^{i} \simeq i^{2/3}\xi_e; \qquad {Q_{tr}}^{i} \simeq i^{1/3}q_e \tag{67}$$

where macroscopic coacervate, neutral aggregates, and charged colloids and PEs are predicted to coexist.

In the following sections, the PE parameters, f and N, and the colloid charge, Q, are considered independent variables, and the only limitation is that $fN \geq Q$.

7. OSMOTIC MODULUS OF COLLOID-POLYELECTROLYTE COACERVATES

The internal structure of the hybrid coacervates proposed here allows us to predict their viscoelastic properties. We start with the osmotic compressibility of the coacervates and employ an

https://doi.org/10.1021/acs.macromol.2c02464
Macromolecules 2023, 56, 1713–1730

approach used by Semenov, Joanny, and Khokhlov for bridged micellar gels of neutral associating polymers.[38] This approach invokes the theory of (generally speaking, nonpolymer) linear elasticity and suggests that the osmotic modulus of the coacervate, K, can be estimated from the free energy change under uniform coacervate compression

$$\Delta\mathcal{F} \simeq \mathcal{V}K\epsilon^2 \tag{68}$$

Here $\mathcal{V}$ is the macroscopic volume of the coacervate and ϵ is the degree of coacervate compression. The K value can be obtained from microscopic considerations of the deformation of the coacervate electroneutral cell, namely, from more detailed considerations of bridging interactions.

7.1. Strong Spherical Adsorption (Regime I). To estimate the osmotic modulus of the gel, we must not only calculate the depth of the free energy minimum due to corona interpretation, which is given by eq 41, but also its steepness. Now δ_I is the (generally speaking, nonequilibrium) depth of coronae interpenetration. The entropic gain due to bridging is equal to $F^I_{br} \simeq -A_I/{\xi_{out}}^2 \simeq -H_I\delta_I/\xi_e^2$ and increases with increasing δ_I. However, corona overlap results in increasing short-range repulsions. The volume of the interpenetration region is $A_I\delta_I$, and the corresponding free energy is equal to the number of blobs in it, $F^I_{rep} \simeq A_I\delta_I/{\xi_{out}}^3 \simeq H_I{\delta_I}^2/{\xi_e}^3$. The resulting free energy

$$F^I_{tot}(\delta_I) = F^I_{br} + F^I_{rep} \simeq \frac{H_I}{{\xi_e}^3}({\delta_I}^2 - \delta_I\xi_e) \tag{69}$$

exhibits a minimum at $\delta_I \simeq \xi_e$, as suggested by eq 40, and the minimum depth is given by eq 41. In the vicinity of this minimum, the free energy can be expanded in a series[38]

$$\begin{aligned} F^I_{tot}(\epsilon) &\simeq -\frac{H_I}{\xi_e} + \frac{1}{2}\frac{H_I}{{\xi_e}^3}(\delta_I - \xi_e)^2 + \ldots \\ &\simeq -\frac{H_I}{\xi_e} + \frac{1}{2}\frac{{H_I}^3}{{\xi_e}^3}\epsilon^2 + \ldots \end{aligned} \tag{70}$$

and deformations remain small (linear) for δ_I less than or of order ξ_e, that is, for $\epsilon \simeq \delta_I/H_I \lesssim \xi_e/H_I$. When the coacervate is compressed by external forces, the change of the total free energy is proportional to the number of electroneutral cells (which is of the same order as the number of contacts between them) in the macroscopic volume $\mathcal{V}$:

$$\Delta\mathcal{F} \simeq \frac{\mathcal{V}}{{H_I}^3}\Delta F^I_{tot} \simeq \frac{\mathcal{V}}{{H_I}^3}\frac{{H_I}^3}{{\xi_e}^3}\epsilon^2 \simeq \mathcal{V}\frac{\epsilon^2}{{\xi_e}^3} \tag{71}$$

Comparison between this result and eq 68 implies that the osmotic modulus of the coacervate in regime I is given by

$$K_I \simeq {\xi_e}^{-3} \simeq uf^2 \tag{72}$$

The linear osmotic compressibility of the colloid−PE complex is therefore defined by the structure of the outer part of the elementary cell,[38] namely, by the size of the outmost blob equal to the electrostatic blob size, $\xi_{out} \simeq \xi_e$.

7.2. Strong Quasi-planar Adsorption (Regime II). For quasi-planar adsorption, $H_{II} \ll R$, the above analysis remains applicable, but the corona thickness H_I should be substituted by the radius of the particle, R. These modifications do not affect the final result

$$K_{II} \simeq {\xi_e}^{-3} \simeq uf^2 \tag{73}$$

Similarly, elasticity of hybrid coacervates in regimes I and II is due to an analogous structure of an outmost blob layer of the elementary cell, $\xi^I_{out} \simeq \xi^{II}_{out} \simeq \xi_e$. In the strong adsorption regimes, I and II, the osmotic modulus of the colloid−PE coacervate derived here coincides with that of the respective symmetric PE−PE coacervate.

7.3. Weak Quasi-planar Adsorption (Regime III). In this regime, the corona thickness and the interpenetration depth are of the same order of magnitude, $\delta_{III} \simeq H_{III}$, and $F^{III}_{br} \simeq -RH_{III}/S_{loop}$. This result means that the change of the free energy per one corona−corona contact is equal to

$$\Delta F^{III}_{tot} \simeq \frac{|F_{br}|}{H^2_{III}}(\epsilon R)^2 \simeq \frac{R^3}{H_{III}S_{loop}}\epsilon^2 \tag{74}$$

The resulting increase in the coacervate free energy

$$\Delta\mathcal{F} \simeq \frac{\mathcal{V}}{R^3}\Delta F^{III}_{tot}(\epsilon) \simeq \mathcal{V}\frac{\epsilon^2}{H_{III}S_{loop}} \tag{75}$$

leads to the following value of the osmotic modulus:

$$K_{III} \simeq u\sigma^2 \simeq u\frac{Q^2}{R^4} \tag{76}$$

This result can also be derived by considering the Coulomb free energy of repulsions between neighboring colloids, $W^{III}_{Coul}(r) \simeq uQ^2/r$ with $r = R + H_{III}$ at equilibrium. Under compression, the distance between the ball centers shortens by ϵR, and the Coulomb free energy increase is given by

$$\Delta W^{III}_{Coul} \simeq \frac{\mathrm{d}^2W_{Coul}}{\mathrm{d}^2r}(\epsilon R)^2 \simeq u\frac{Q^2}{R^3}(\epsilon R)^2 \simeq u\frac{Q^2}{R}\epsilon^2 \tag{77}$$

with $\epsilon \lesssim H_{III}/R$. Since $\Delta W^{III}_{Coul} \simeq \Delta F^{III}_{tot}$, one arrives at the final result given by eq 76.

One can compare these results for the osmotic modulus in the regimes of weak and strong quasi-planar adsorption. The disparity between $K_{III} \simeq uQ^2/R^4$ and $K_{II} \simeq {\xi_e}^{-3}$ shows that the compression of the hybrid coacervate in different regimes is associated with different energy and length scales. For the strong adsorption regime II, coacervate deformation only leads to the reorganization of the narrow interfacial layer of the electroneutral cell, with thickness equal to the outmost blob size, ξ_e; the characteristic energy per blob is comparable to the thermal energy. In regime III, the weakly adsorbed layer is sparse, and external deformation makes Coulomb repulsions between colloids not entirely screened by the PEs; the respective energy far exceeds k_BT. Technically, a comparison between eq 70 written for regime II (that is, with H_I substituted by R) and eq 77 describing regime III explains why K_{III} can be obtained from K_{II} upon renormalization of the corresponding energies and lengths, $1 \to uQ^2/R$ and $\xi_e \to R$.

8. LINEAR VISCOELASTICITY OF COLLOID-POLYELECTROLYTE COACERVATES

In Section 6, the constraint of charge matching of colloids and PEs, $Q = fN$, has been released. Here we consider arbitrarily long PEs with $N > Q/f$. Since the increasing PE length has a negligible effect on the internal structure of hybrid coacervates, we use the results of Section 4 for the coacervate density in Regimes I−III.

8.1. Strong Spherical Adsorption (Regime I). In regime I, most of the volume of the hybrid coacervate is occupied by PEs, and the rheological properties are polymer-controlled. Neglecting the internal inhomogeneity of the PE shell, which is

https://doi.org/10.1021/acs.macromol.2c02464
Macromolecules 2023, 56, 1713−1730

discussed in Appendix A, hybrid coacervates can be considered as a semidilute polymer solution with the (average) polymer volume fraction ϕ_I and (average) correlation length

$$\xi_I \simeq \phi_I^{-1} \simeq u^{-3/5} f^{-4/5} Q^{-2/5} \tag{78}$$

The constraint $\sigma \ll \sigma_{ion}$ given by eq 52 implies that the energy of Coulomb interactions is lower than k_BT per charge. This leads to the absence of any electrostatic activation barriers and hence nonsticky dynamics for the PEs. To prove this statement, we demonstrate that, even at $\sigma \simeq \sigma_{ion} \simeq u^{-1/2} f^{3/4}$, the activation energy for the detachment of a single charge from the colloid interface, E_a, is lower than the thermal energy. In this case, the size of the blob closest to the interface equals $\xi_{prox} \simeq u^{-1/3} \sigma_{ion}^{-2/3} \simeq f^{-1/2}$, see eq A7. This result shows that there is, on average, one charge in the closest blob,[27,28] and the respective activation energy is the product of the blob size and the value of the electric field near the particle interface, $E_a \simeq f^{-1/2} u \sigma_{ion} \simeq u^{1/2} f^{1/4}$. The absence of any activation processes, $E_a \ll 1$, is provided by eq 9, which also ensures the absence of strong charge correlations and ion pairing in the respective conventional coacervates.[22,23,50,51]

Chain conformations within the PE shell are not perturbed by Coulomb interactions and can be viewed as those for a quasineutral semidilute solution.[24] This enables applying standard Rouse and reptation models of polymer dynamics[52] for estimating the longest relaxation time and viscosity of the hybrid coacervates. For relatively short chains, results for the Rouse model for neutral semidilute solution yield

$$\tau_{Rouse}^I \simeq \tau_0 \phi_I N^2 \simeq \tau_0 u^{3/5} f^{4/5} Q^{2/5} N^2 \tag{79}$$

$$\eta_{Rouse}^I \simeq \eta_s \phi_I^2 N \simeq \eta_s u^{6/5} f^{8/5} Q^{4/5} N \tag{80}$$

Here η_s is the solvent viscosity and $\tau_0 = \eta_s b^3/k_BT$ is the monomer relaxation time.

In a Θ solvent, chains become entangled when the PE length N exceeds[52,53]

$$N_{Rouse/rep}^I \simeq \phi_I^{-4/3} N_e \simeq u^{-4/5} f^{-16/15} Q^{-8/15} N_e \tag{81}$$

with N_e being equal to the length of the entanglement strand in the melt. Long chains exhibit reptation dynamics, with

$$\tau_{rep}^I \simeq \tau_0 \phi_I^{7/3} \frac{N^3}{N_e} \simeq \tau_0 u^{7/5} f^{28/15} Q^{14/15} \frac{N^3}{N_e} \tag{82}$$

$$\eta_{rep}^I \simeq \eta_s \phi_I^{14/3} \frac{N^3}{N_e^2} \simeq \eta_s u^{14/5} f^{56/15} Q^{28/15} \frac{N^3}{N_e^2} \tag{83}$$

The assumption of the dominant contribution of the PEs to the Newtonian viscosity of hybrid coacervates can be proven. To this end, the contribution to the viscosity due to the nanoparticles can be calculated and compared to that due to the polymers. First, we consider the case of short PEs (Rouse dynamics) and/or small particles with a size much smaller than the reptation tube diameter, $R \ll a \simeq N_e^{1/2} \phi^{-2/3}$.[52] We follow the approach of refs 54, 55. to estimate the mobility of the colloidal particles. The effective viscosity experienced by the nanoparticle is defined by the viscosity of the semidilute solution *at length scales comparable to the nanoparticle size*, R.[54,55] The number of monomers in the PE strand of size R is given by $g_R \simeq R^2$ because polymers exhibit Gaussian statistics at all length scales. *The effective viscosity* of the polymer solution, which is experienced by the nanoparticle, is equal to the Rouse viscosity of the semidilute solution of chains containing g_R monomers:

$$\eta_{eff}(R) \simeq \eta_s \phi_I^2 g_R \simeq \eta_s \phi_I^2 R^2 \tag{84}$$

The resulting diffusion coefficient of the nanoparticle is given by

$$D_{np}^{unent} \simeq \frac{k_BT}{R\eta_{eff}(R)} \simeq \frac{k_BT}{\eta_s \phi_I^2 R^3} \simeq D_0 u^{-6/5} f^{-8/5} Q^{-4/5} R^{-3} \tag{85}$$

and rapidly decreases with increasing R, demonstrating that large particles experience substantially higher friction.[54,55] Here $D_0 = k_BT/\eta_s b$ is the diffusion coefficient of a single disjointed monomer (and b in the denominator appears due to R expressed in the units of b). The relaxation time of the nanoparticle is equal to the time required to diffuse by a distance of order R:

$$\tau_{np} \simeq \frac{R^2}{D_{np}} \simeq \tau_0 \phi_I^2 R^5 \simeq \tau_0 u^{6/5} f^{8/5} Q^{4/5} R^5 \tag{86}$$

The value of the relaxation modulus at $t = \tau_{np}$ can be found by assuming that each nanoparticle has of order one unrelaxed mode and that the concentration of colloids is equal to ϕ_I/H_I^3:

$$G|_{t=\tau_{np}(R)} \simeq k_BT \frac{\phi_I}{H_I^3} \tag{87}$$

The colloidal contribution to the viscosity is given by the product of the relaxation time and the modulus value at the relaxation time:

$$\eta_{np}^I \simeq \tau_{np}(R) \cdot G|_{t=\tau_{np}(R)} \simeq \tau_0 \phi_I^3 \frac{R^5}{H_I^3} \tag{88}$$

The relative contribution to the viscosity from the nanoparticles is negligible

$$\frac{\eta_{np}^I}{\eta_{Rouse}^I} \simeq \phi_I \frac{R^2}{N} \left(\frac{R}{H_I}\right)^3 \ll 1 \tag{89}$$

owing to the low values of each of the three multipliers in eq 89: $\phi_I \ll 1$ due to low coacervate densities, $R \ll H_I$ because the PE shell is thick in regime I, and $R^2/N \le R^2 f/Q \ll 1$ according to eq 19.

A similar analysis can be performed for large particles, with a radius that exceeds substantially the diameter of the entanglement tube, $R \gg a \simeq N_e^{1/2} \phi_I^{-2/3}$.[54,55] Entangled particles "feel" a viscosity equal to that of the entangled quasineutral semidulite solution of polyanions, $\eta_{eff}(R) \simeq \eta_{rep}^I$, which is given by eq 83. Their diffusion coefficient reads

$$D_{np}^{ent} \simeq \frac{k_BT}{R\eta_{rep}^I} \simeq D_0 u^{-14/5} f^{-56/15} Q^{-28/15} R^{-1} N_e^2 N^{-3} \tag{90}$$

and results in a particle relaxation time

$$\tau_{np} \simeq \frac{R^2}{D_{np}} \simeq \frac{\eta_{rep}^I R^3}{k_BT} \simeq \tau_0 u^{14/5} f^{56/15} Q^{28/15} R^3 \frac{N^3}{N_e^2} \tag{91}$$

Using the value of the modulus at the nanoparticle relaxation time given by eq 87, one arrives at the colloidal viscosity contribution

$$\eta_{np}^I \simeq \eta_{rep}^I \phi_I \left(\frac{R}{H_I}\right)^3 \tag{92}$$

which is small as compared to the polymer contribution, η_{rep}^I. We finally note that the above analysis of nanoparticle mobility and

https://doi.org/10.1021/acs.macromol.2c02464
Macromolecules 2023, 56, 1713−1730

contribution to the viscosity was performed for the limiting cases of $R \ll a$ and $R \gg a$. This results in a sharp crossover between these regimes and, for example, the jump in the colloidal viscosity contribution (cf. eqs 88 and 92 at $R \simeq a$). Taking into account the hopping mechanism encountered in nanoparticle diffusion in semidilute solutions with $a \simeq R$ would widen and smooth this crossover.[56]

To summarize, the above analysis underscores the consistency of our results for the coacervates' viscosity, which in regime I is dominated by the PEs. The respective results for the coacervate viscosity in an athermal solvent are provided in Appendix B.

It is of interest to compare the results above with those for symmetric PE−PE complex coacervates, τ^{sym} and η^{sym}. The latter can be obtained using eqs 79−83 by substituting the hybrid coacervate density with that of its PE−PE counterpart, $\phi_I \to \phi_e \simeq (uf^2)^{1/3}$.[24,57] Hybrid coacervates are more viscous

$$\frac{\eta_R^I}{\eta_R^{sym}} \simeq \left(\frac{Q}{q_e}\right)^{4/5} \gg 1 \tag{93}$$

$$\frac{\eta_{rep}^I}{\eta_{rep}^{sym}} \simeq \left(\frac{Q}{q_e}\right)^{28/15} \gg 1 \tag{94}$$

and exhibit longer relaxation times, $\tau_R^I/\tau_R^{sym} \simeq (Q/q_e)^{2/5} \gg 1$ and $\tau_{rep}^I/\tau_{rep}^{sym} \simeq (Q/q_e)^{14/15} \gg 1$, which can be attributed solely to their higher densities. For the same reason, the crossover from Rouse to reptation dynamics in colloid−PE coacervates takes place at shorter polymer lengths, $N_{R/rep}^I/N_{R/rep}^{sym} \simeq (q_e/Q)^{8/15} \ll 1$. We note that the rheological properties of hybrid coacervates can be assessed not only directly, by measuring their Newtonian viscosity and relaxation moduli, but also indirectly, by tracking the diffusion of the nanoparticles using e.g. fluorescence correlation spectroscopy (FCS) or X-ray photon correlation spectroscopy (XPCS). Equations 85, 86 and 90, 91 demonstrate that their diffusion coefficients and relaxation times are very sensitive to both their size/charge and the properties of the PEs and the solvent environment.

8.2. Quasi-planar Adsorption (Regimes II and III). In regimes II and III, a substantial part of the hybrid coacervate volume is occupied by the nanoparticles, and their volume fraction $\Phi \simeq 1$. The naive approach would be to simply substitute the average density of the PE layer ϕ_I with the respective ϕ_{II} and ϕ_{III} values in the above analysis. However, we expect that the viscosity of the coacervate in these regimes may be not entirely dominated by polymers (see eq 89) and strongly influenced by the colloids. For instance, for the simplest model of the colloidal suspension—hard-sphere-like colloids in simple (nonpolymer) solvent—the Newtonian viscosity steeply increases in the vicinity of $\Phi \geq 0.5$,[58−60] which signals a glass and/or jamming transition. The primary physical reason for that is caging of the nanoparticles at high densities.[61] When the density reaches $\Phi_{RCP} = 0.63$, the system transitions into a random close-packed (RCP) solid. Therefore, a nonpower-law dependence of η on Φ can be expected in the quasi-planar regimes. Moreover, the rheological behavior of dense suspensions of nanoparticles may also depend on their mechanical properties, that is, differ for the cases of soft and solid spheres (e.g., globular proteins versus solid colloids), smooth and rough particle surfaces, etc. For this reason, we do not provide scaling estimates in terms of the parameters introduced here for the hybrid coacervate viscosity in this regime. This problem should be addressed in future work.

9. CONCLUSIONS AND DISCUSSION

A scaling theory of structure and linear viscoelasticity of hybrid coacervates formed from polyelectrolytes and oppositely charged spherical colloids has been developed. An electroneutral cell for the hybrid coacervate can be viewed as consisting of a colloid covered by an adsorbed polyelectrolyte shell, with attractions between elementary cells provided by entropic bridging interactions. The coacervate structure is defined by the adsorption strength and thickness of the adsorbed layer. A scaling diagram of hybrid coacervation is presented in Figure 4 for the Θ solvent case and in Figure B1 for athermal solutions.

We distinguish the scaling regimes of (I) strong spherical adsorption, (II) strong quasi-planar adsorption, and (III) weak quasi-planar adsorption. In the strong adsorption regimes, I and II, the density profile of the adsorbed layer is controlled by the balance between Coulomb attractions and short-range repulsions. The polyelectrolyte shell is inhomogeneous, with a density that decreases from the particle interface to the periphery. Its average density exceeds that of conventional polyelectrolyte-polyelectrolyte coacervates, i.e., it is higher than that within the electrostatic blob. In regime III of weak adsorption, colloid-polyelectrolyte Coulomb attractions are balanced by the conformational entropy of the compressed polyelectrolytes.

The adsorbed layer adopts essentially a spherical geometry and its thickness is large, $H \gg R$, in regime I when the charge of the colloid is high and/or its radius is small. In contrast, at lower Q and higher R, the polyelectrolyte shell is thin, $H \ll R$, and these regimes, II and III, are termed quasi-planar.

The osmotic compressibility of hybrid coacervates is defined by the structure of the adsorbed polyelectrolyte shell. In Regimes I and II, it consists of many layers of blobs, and Coulomb interactions between the colloids are strongly screened by the shells. The coacervate deformation perturbs only the outmost blobs of the shell, whose size is equal to the electrostatic blob size. The osmotic modulus of the coacervate, $K_I \simeq K_{II} \simeq 1/\xi_e^3 \simeq uf^2$, is therefore independent of the colloids' properties and is equal to that of the conventional polyelectrolyte complex coacervate, which can be viewed as a melt of oppositely charged electrostatic blobs. In contrast, in regime III, the polyelectrolyte shell is sparse and the coacervate deformation leads to bare Coulomb repulsions between the colloids. The latter results in an osmotic modulus $K_{III} \simeq uQ^2R^{-1}/R^3 \simeq uQ^2/R^4$, which increases with colloid charge and with decreasing size. These predictions can be experimentally tested in scattering studies of hybrid coacervates by measuring their osmotic compressibility, $S(q)$ for $q \to 0$.

The surface tension of hybrid coacervates is due to bridging interactions between neighboring shells, specifically, their outer parts. It is controlled by the area and depth of the shell's interpenetration. The latter is of the same order as the outmost blob size, and much smaller than the total shell thickness when adsorption is strong (Regimes I and II). For weak adsorption (regime III), when the adsorbed layer consists of rare loops of polyelectrolytes rather than the layers of densely packed adsorption blobs, shells interpenetrate entirely. For any regime, the surface tension of hybrid colloid-polyelectrolyte coacervates is low in comparison to that of their conventional interpolyelectrolyte counterparts. In regime I, when $H \gg R$, most of the coacervate volume is occupied by polyelectrolytes; the average

https://doi.org/10.1021/acs.macromol.2c02464
Macromolecules 2023, 56, 1713−1730

density of the shell and the average polyelectrolyte density within the hybrid coacervate are close to each other. Remarkably, in this regime, hybrid coacervates have simultaneously a lower surface tension but higher average density than their corresponding polyelectrolyte-polyelectrolyte analogs. This feature should be attributed to the inhomogeneous structure of the polyelectrolyte shell.

We predict that the rheological properties of the coacervates are dominated by the polyelectrolytes when they are sufficiently long, $fN > Q$, and the shell thickness is high (regime I). To describe polymer dynamics, a polyelectrolyte shell can be viewed as a quasi-neutral semidilute solution of neutral polymers and its density heterogeneity can be neglected. By applying classical Rouse and reptation models for unentangled and entangled solutions, respectively, one can derive expressions for the relaxation times of polyanions, eqs 79 and 82, and for the coacervate viscosity, eqs 80 and 83. These results are extended to athermal solvents in Appendix B, eqs B18 and B20. The relaxation times and viscosity are increasing functions of the colloid charge, Q, because the coacervate density is higher for higher Q values, but is independent of the particle radius. Hybrid coacervates are more viscous than traditional complex coacervates (eqs 93 and 94). These results hold when charge correlations are weak, polyelectrolytes do not stick to the colloid interface, and the coacervate is liquid, rather than gel-like.

The diffusion coefficients of the colloids within the hybrid coacervate are rapidly decreasing functions of their charge and radius. For instance, under Θ solvent conditions, $D_{np}^{unent} \sim Q^{-4/5}R^{-3}$ for colloids smaller than the reptation tube diameter and $D_{np}^{ent} \sim Q^{-28/15}R^{-1}$ for much larger, entangled colloids. The respective results in an athermal solvent are given by eqs B21 and B22. These results can be experimentally examined using fluorescence correlation spectroscopy (FCS). The relaxation times of nanoparticles have been obtained, which permits calculation of their contribution to the Newtonian viscosity. The latter is negligible when compared to the polymer contribution until the shell is thin, $H \simeq R$. This demonstrates the consistency of our viscoelasticity analysis for coacervates with thick polyelectrolyte shells, regime I.

In regimes II and III, when the shell is thin and colloids are the major (by volume) constituent of hybrid coacervates, the rheology is expected to be sensitive not only to the colloid charge and size, Q and R, but also to their mechanical properties such as stiffness/elasticity, surface roughness, and the friction between them. For instance, solid nanoparticles are very rigid while globular proteins and surfactant micelles are much softer and more compliant. Therefore, this regime may be not adequately described within our minimal two-parametric (Q, R) model of the colloid, which entirely neglects its internal structure and viscoelastic properties.

We believe that this work provides helpful theoretical insights into the mechanism of formation, structure, and rheology of colloid-polyelectrolyte coacervates. Our findings may serve as useful guidelines for the targeted design of hybrid coacervate-based materials.

9.1. Comparison to Protein-RNA Experiments. In recent experiments, Obermeyer and co-workers studied coacervation between supercationic globular green fluorescent proteins (GFPs) of different charges and anionic RNA. It was observed that the GFP charge, Q, is a key determinant of hybrid complex coacervation and protein diffusion in the condensed phase. Phase separation was absent *in vitro* at any protein and RNA concentration when the GFP charge was low, $Q/e = +12$. For $Q/e = +16$; complex coacervation took place only at high concentrations of GFP and RNA. Finally, as the charge increased further to $Q/e = +36$, the two-phase region on the phase diagrams extended to much lower concentrations. A similar trend was also revealed in *in vivo* studies, where increasing Q facilitated intracellular phase separation and the formation of subcellular assemblies.[11] These results are consistent with our theoretical predictions, shown in the scaling diagrams for hybrid complex coacervation, Figures 4 and B1, which suggest the absence of phase separation at low protein charge Q. At higher Q values, in regimes I–III, coacervation takes place above the threshold concentration c_{coac}, which, according to eqs 61–63, rapidly decreases with increasing charge Q.

Fluorescent recovery after photobleaching showed that the GFP diffusion between different cellular compartments is a decreasing function of Q.[11] This is in qualitative agreement with eqs 85 and 90, which predict that the diffusion coefficient of colloids goes down with increasing charge.

In view of the relatively high linear charge density of RNA, the strict applicability of our theory to GFP-RNA hybrid coacervates may be limited. In order to quantitatively corroborate the predictions provided here, one may substitute RNA with PEs carrying a lower linear charge density. For instance, the copolymer of neutral ethylene oxide and ionically functionalized allyl glycidyl ether can be used. The synthesis of these coPEs, which contain as little as 30% of ionic monomers, and their conventional (interpolyelectrolyte) coacervation, were reported in ref 14. Assuming that the statistical segment length for this copolymer is close to that for poly(ethylene oxide), $b \approx 1$ nm, the fraction of the segments carrying charge is $f \approx 1$. In an aqueous medium, the Bjerrum length $l_b \approx 0.7$ nm and, in dimensionless units, equals $u = l_b/b \approx 0.7$. The radius of the GFP is about 1.5 nm, which leads to $R \approx 1.5$ when it is expressed in units of b. In this case, the crossover I/II reads $Q_{I/II}/e \simeq uf^3R^5 \approx 5.3$, suggesting that the hybrid coacervates formed from the supercharged GFP with $Q/e = 12$, 16, and 36 should likely belong to regime I. This system would enable testing both the structural and rheological predictions provided herein. It should be noted, however, that this estimate is approximate because the numerical coefficients in all scaling crossovers are unknown. Analogous estimates for GFP-RNA hybrid coacervates show that they are rather in regime II, but high u and f values lead to such theoretically disregarded effects like electrostatic stiffening of ssRNA and may limit the rigorous applicability of our results.

APPENDIX A

A. Inhomogeneous Internal Structure of Strongly Adsorbed Layers

In regimes I and II of strong adsorption, the adsorbed layer is the densely packed array of blobs, as shown in Figure A1. We denote $\xi(r)$ the size of the blob, and $\phi(r) \simeq 1/\xi(r)$ is the polymer volume fraction inside it.

There are three forces acting on each of the blobs in the radial direction. Two of them are due to the pressure (provided by the short-range repulsion of monomers) of the neighboring inner and outer blob layers, and the third one is the Coulomb force of interaction with the partially screened ball. The osmotic pressure within the semidilute solution, which consists of the blobs of $\xi(r)$ size, scales as $1/\xi^3(r)$. The radial force balance for the blob reads

https://doi.org/10.1021/acs.macromol.2c02464
Macromolecules 2023, 56, 1713−1730

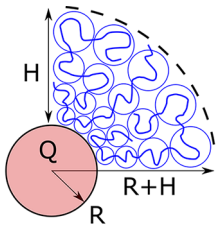

Figure A1. Internal structure of the strongly adsorbed layer: The array of the densely packed blobs of $\xi(r)$ size, which increases with increasing r.

$$\xi^2(r)\left(\frac{1}{\xi^3(r)} - \frac{1}{\xi^3(r+\xi(r))}\right) \simeq q(r)E(r) \tag{A1}$$

Here $q(r) \simeq fg(r) \simeq f\phi^{-2}(r)$ is the charge of the blob, and the value of the electric field $E(r)$ at the distance r from the center is given by

$$E(r) \simeq \frac{uQ(r)}{r^2} \simeq \frac{u}{r^2}\left(Q - \int_R^r f\phi(r)r^2\mathrm{d}r\right) \tag{A2}$$

The resulting integral equation defining the density profile $\phi(r)$ of the PE shell has the following form

$$-\frac{\mathrm{d}}{\mathrm{d}r}(\phi^2(r)) \simeq \frac{uf}{r^2}\left(Q - \int_R^r f\phi(r)r^2\mathrm{d}r\right) \tag{A3}$$

with $R \le r \le R + H$. This equation should be solved with account for the electrical neutrality constraint:

$$\int_R^{R+H} f\phi(r)r^2\mathrm{d}r = Q \tag{A4}$$

The boundary condition $\phi(R + H) = 0$ requires zero polymer density at the shell edge.

Since eq A3 cannot be solved analytically in the general case, one should consider the limiting cases of quasi-planar (regime II) and essentially spherical (regime I) adsorption.

A.1. Quasi-planar Layer (Regime II). Neglecting the curvature of the shell for $H \ll R$ and assuming $r \simeq R$ in eq A3, one arrives at

$$\frac{\mathrm{d}^2}{\mathrm{d}r^2}(\phi^2(r)) \simeq uf^2\phi(r) \tag{A5}$$

With an account for the boundary and normalization (i.e., pair neutrality) conditions, the resulting polymer density profile reads:[28]

$$\phi_{II}(r) \simeq uf^2(R + H_{II} - r)^2 \simeq uf^2(H_{II} - h)^2 \tag{A6}$$

with $h = r - R$ being the distance from the ball surface and the total layer thickness $H_{II} \simeq u^{-1/3}f^{-1}\sigma^{1/3}$, in accordance with eq 15. The size of the most proximate blob

$$\xi_{prox}^{II} \simeq u^{-1/3}\sigma^{-2/3} \tag{A7}$$

coincides with the average blob size within the layer because the average layer density equals $\phi_{II} \simeq u^{1/3}\sigma^{2/3}$, in agreement with eq 16.

The size of the outmost blob can be found from the closure $\phi(h) \simeq \xi^{-1}(h)$ for $h = H - \xi_{out}$:

$$\xi_{out}^{II} \simeq (uf^2)^{-1/3} \simeq \xi_e \tag{A8}$$

This result demonstrates that the outmost blob is equal to the electrostatic blob.[28] It is important for proper consideration of bridging interactions.

A.2. Spherical Layer (Regime I). In this case, the outer part of the shell can be considered as a quasi-planar adsorbed layer surrounding the ball with the renormalized (partially screened by the inner part of the coat) charge Q^*. Therefore, the result

$$\xi_{out}^{I} \simeq (uf^2)^{-1/3} \simeq \xi_e \tag{A9}$$

remains unchanged because it is independent of Q; it is used for the calculations of the bridging free energy.

To find the thickness of the shell in regime II, one can substitute the planar solution given by eq A6 into the global neutrality constraint, eq A4. This yields the shell thickness $H_I \simeq u^{-1/5}f^{-3/5}Q^{1/5}$ consistent with eq 3.

Another way to estimate the shell thickness is to consider the inner part of the shell where the screening of the ball charge by the shell is negligible, i.e., to assume $Q(r) \simeq Q$ in eq A3. The resulting equation for the density profile

$$-\frac{\mathrm{d}}{\mathrm{d}r}(\phi^2(r)) \simeq \frac{ufQ}{r^2} \tag{A10}$$

has the solution

$$\phi_{thick}(r) \simeq \left[ufQ\frac{(H - r)}{Hr}\right]^{1/2} \tag{A11}$$

satisfying the boundary condition $\phi(R + H) \simeq \phi(H) = 0$. Substituting this approximate density profile into eq A4 one can obtain the equation defining the shell thickness:

$$u^{1/2}f^{3/2}Q^{1/2}\int_0^H \left(\frac{H - r}{Hr}\right)^{1/2} r^2\mathrm{d}r \simeq u^{1/2}f^{3/2}Q^{1/2}H^{5/2} \simeq Q \tag{A12}$$

We finally arrive at $H_I \simeq u^{-1/5}f^{-3/5}Q^{1/5}$, in accordance with eq 3.

APPENDIX B

B. Hybrid Coacervates in Athermal Solvent

The analysis performed in the main text can be extended from Θ solvent to athermal solvent. In the latter case, PE conformations at short length scales have swollen coil statistics with the scaling exponent $\nu = 0.588$. In what follows, we express our result as the function of ν. We note that, for $\nu = 1/2$, all results (except for the entangled coacervate viscosity and colloid mobility in it) exactly reproduce those for Θ solvent, which are derived in the main text.

The size and charge of the electrostatic blob in athermal solvent are given by

$$\xi_{e+} \simeq (uf^2)^{-\nu/(2-\nu)} \tag{B1}$$

$$q_{e+} \simeq fg_{e+} \simeq (uf^{\nu})^{-1/(2-\nu)} \tag{B2}$$

The scaling picture of the hybrid coacervates in all regimes remains unchanged, and the only difference is that short-range repulsions between monomers in athermal solvent are provided by two-body rather than three-body interactions.

B.1. Strong Spherical Adsorption (Regime I+). In regime I+, the energy of Coulomb interactions is given by eq 1 and reads $F_{Coul}^{I+} \simeq -uQ^2/H$. The energy of excluded volume interactions can be estimated as k_BT per one blob, $F_{vol}^{I+} \simeq V/\xi^3 \simeq H^3(Q/fH^3)^{3\nu/(3\nu-1)}$. Here we have neglected the inhomogeneity of the shell and used the standard closure

https://doi.org/10.1021/acs.macromol.2c02464
Macromolecules 2023, 56, 1713−1730

between the average blob size and polymer volume fraction in it, $\xi \simeq \phi^{-\nu/(3\nu-1)}$. The balance between Coulomb attractions and short-range repulsions results in the shell thickness and average density given by

$$H_{I+} \simeq \left(\frac{Q^{2-3\nu}}{u^{3\nu-1}f^{3\nu}}\right)^{1/(4-3\nu)} \tag{B3}$$

$$\phi_{I+} \simeq (u^3 f^4 Q^2)^{(3\nu-1)/(4-3\nu)} \tag{B4}$$

More careful analysis can be performed to demonstrate that the size of the outmost blob in the shell is equal to the electrostatic blob size, $\xi_{out} \simeq \xi_{e+}$, by analogy with the case of Θ solvent discussed in Appendix A. This leads to the energy of bridging interactions given by $F_{br}^{I+} \simeq -H_{I+}/\xi_{e+}$. The coacervate surface tension can be calculated as $\gamma_{I+} \simeq |F_{br}^{I+}|/H_{I+}^2 \simeq 1/H_{I+}\xi_{e+}$:

$$\gamma_{I+} \simeq \frac{u^{(11\nu-6\nu^2-2)/((2-\nu)(4-3\nu))} f^{\nu(14-9\nu)/((2-\nu)(4-3\nu))}}{Q^{(2-3\nu)/(4-3\nu)}} \tag{B5}$$

B.2. Strong Quasi-planar Adsorption (Regime II+). According to eq 13, the energy of Coulomb attractions between the nanoparticle and quasi-planar layer equals $F_{Coul}^{II+} \simeq uQ^2H/R^2$. Their balance with short-range repulsions, $F_{vol}^{II+} \simeq V/\xi^3 \simeq HR^2(Q/fHR^2)^{3\nu/(3\nu-1)}$, results in the following laws for the shell properties:

$$H_{II+} \simeq \frac{\sigma^{(2-3\nu)/3\nu}}{u^{(3\nu-1)/3\nu}f} \simeq \frac{(Q/R^2)^{(2-3\nu)/3\nu}}{u^{(3\nu-1)/3\nu}f} \tag{B6}$$

$$\phi_{II+} \simeq (u\sigma^2)^{(3\nu-1)/3\nu} \simeq \left(\frac{uQ^2}{R^4}\right)^{(3\nu-1)/3\nu} \tag{B7}$$

Equations B6 and B7 are consistent with the results of Dobrynin[62] who considered adsorption of PEs on the planar charged surface in athermal solvent. For the quasi-planar regimes, the properties of the adsorbed layer depend only on the effective charge density of the ball, $\sigma \simeq Q/R^2$.

Since the size of the outmost blob in the adsorbed layer is equal to the electrostatic blob size, $\xi_{out} \simeq \xi_{e+}$, the energy of bridging interactions is $F_{br}^{II+} \simeq -R/\xi_{e+}$. This leads to the coacervate surface tension $\gamma_{II+} \simeq |F_{br}^{II+}|/R^2 \simeq 1/R\xi_{e+}$, or equivalently

$$\gamma_{II+} \simeq (uf^2)^{\nu/(2-\nu)}R^{-1} \tag{B8}$$

Crossover between the regimes of spherical and quasi-planar absorption can be found from $H_{I+} \simeq H_{II+} \simeq R$:

$$Q_{I+/II+} \simeq q_{e+}\left(\frac{R}{\xi_{e+}}\right)^{(4-3\nu)/(2-3\nu)} \tag{B9}$$

The numerical value of the exponent for athermal solvent, $(4-3\nu)/(2-3\nu) = 9.47$, differs from the value of 5 for the Θ solvent found in the main text. We note that, if the lengths and charges are expressed in q_e and ξ_e values for the respective solvent quality, this crossover is the only one that depends on the solvent quality, i.e., on the value of ν.

B.3. Weak Quasi-planar Adsorption (Regime III+). In the regime of weak planar adsorption, Coulomb attractions between the nanoparticle and PEs, $F_{Coul}^{III+} \simeq uQ^2H/R^2$, are balanced by entropic forces preventing strong compression of the polymer. The free energy of the compressed PE can be calculated as for the ideal chain of the electrostatic blobs.[25] The latter consists of N/g_{e+} quasi-monomers, and each quasi-monomer has size ξ_{e+}. For ideal Gaussian chain confined within the thin layer of thickness H, the respective conformational free energy would be equal to $F_{conf} \simeq Na^2/H^2$. For the considered PE, we use substitutions $a \to \xi_e$ and $N \to N/g_e$ to obtain $F_{conf}^{III+} \simeq N\xi_{e+}^2/g_{e+}H^2$ where $N = Q/f$. Solving $F_{Coul}^{III+} \simeq F_{conf}^{III+}$ one arrives at[25]

$$H_{III+} \simeq u^{-(1+\nu)/(3(2-\nu))}f^{-\nu/(2-\nu)}\sigma^{-1/3} \simeq \frac{(R^2/Q)^{1/3}}{u^{(1+\nu)/(3(2-\nu))}f^{\nu/(2-\nu)}} \tag{B10}$$

$$\phi_{III+} \simeq \frac{u^{(1+\nu)/(3(2-\nu))}}{f^{2(1-\nu)/(2-\nu)}}\sigma^{4/3} \simeq \frac{u^{(1+\nu)/(3(2-\nu))}}{f^{2(1-\nu)/(2-\nu)}}\left(\frac{Q}{R^2}\right)^{4/3} \tag{B11}$$

Again, the dependence of the shell properties on the nanoparticle radius and charge reduces to that on the charge density σ, as expected for any quasi-planar regime.

To find the free energy gain due to bridging interactions, one should first find the average area of the nanoparticle per one loop, S_{loop}. Each loop contains $n_{loop} \simeq g_{e+}H_{III+}^2/\xi_{e+}^2$ monomers. The charge balance condition for the coacervate electroneutral cell yields $S_{loop} \simeq R^2 f n_{loop}/Q \simeq f g_{e+}H^2/\sigma\xi_{e+}$. Assuming the energy gain k_BT per one loop, one can obtain $F_{br}^{III+} \simeq -H_{III+}/RS_{loop}$ and the resulting surface tension $\gamma_{III+} \simeq |F_{br}|/R^2$:

$$\gamma_{III+} \simeq \frac{u^{(4-5\nu)/(3(2-\nu))}Q^{4/3}}{f^{2\nu/(2-\nu)}R^{11/3}} \tag{B12}$$

The crossover between regimes II+ and III+ can be written as $\sigma \simeq \sigma_{e+}$, where $\sigma_{e+} \simeq q_e\xi_{e+}^{-2}$ is the surface charge density of the electrostatic blob. In the reduced units of the electrostatic blob charge and size, q_{e+} and ξ_{e+}, this crossover takes the form independent of the solvent quality, cf. eq 32:

$$Q_{II+/III+} \simeq q_{e+}\left(\frac{R}{\xi_{e+}}\right)^2 \tag{B13}$$

Here we recall that the electrostatic blob properties are controlled by the solvent quality. The boundary of the coacervation region is defined by $|F_{br}^{III+}| \simeq 1$ and also has ν-independent form similar to eq 48:

$$Q_{coac+} \simeq q_{e+}\left(\frac{R}{\xi_{e+}}\right)^{5/4} \tag{B14}$$

Finally, the adsorption onset coincides with the result of eq 39

$$Q_{ads+} \simeq q_{e+}\left(\frac{R}{\xi_{e+}}\right)^{1/2} \tag{B15}$$

B.4. Scaling Diagram of Coacervation. The results of the performed analysis are summarized in the diagram of the coacervate scaling regimes shown in Figure B1. We note that this diagram is remarkably similar to that for Θ solvent, Figure 4. When the problem parameters are expressed in the reduced units, namely, electrostatic blob size and charge, ξ_{e+} and q_{e+}, all boundaries except for the crossover I/II are universal and not

https://doi.org/10.1021/acs.macromol.2c02464
Macromolecules 2023, 56, 1713−1730

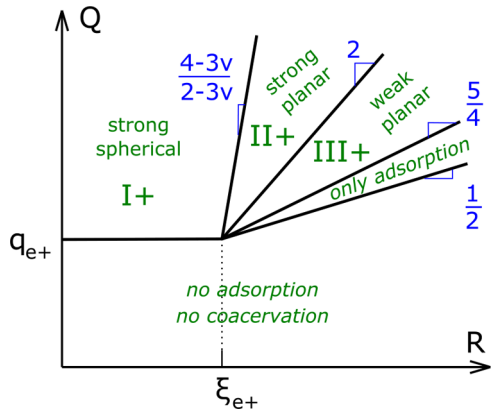

Figure B1. Scaling diagram of hybrid coacervation in athermal solvent, $\nu = 0.588$. The diagram is constructed for the charge-matched system, $fN = Q$.

affected by the solvent quality. Scaling laws for the equilibrium properties of hybrid coacervates in athermal solvent are given in Table B1.

B.5. Coacervate Osmotic Modulus. The value of the osmotic modulus in regimes I+ and II+ are controlled by the size of the outmost blob of the shell, $\xi_{out} \simeq \xi_{e+}$:

$$K_{I+} \simeq K_{II+} \simeq {\xi_{e+}}^{-3} \simeq (uf^2)^{-3\nu/(2-\nu)} \tag{B16}$$

In regime III+, the osmotic modulus is given by eq 76 and is independent of the solvent quality

$$K_{III+} \simeq u\sigma^2 \simeq uQ^2R^{-4} \tag{B17}$$

B.6. Coacervate Viscosity. In regime I+, when most of the condensed phase is occupied by PEs, their dynamics can be described by classical Zimm-Rouse and Zimm-reptation models developed for neutral semidilute solutions.[52] For the short chains demonstrating Rouse dynamics, the viscosity is given by

$$\eta_{Rouse}^{I+} \simeq \eta_s {\phi_{I+}}^{1/(3\nu-1)} N \simeq \eta_s (u^3 f^4 Q^2)^{1/(4-3\nu)} N \tag{B18}$$

and noticeably increases at increasing the Bjerrum length, the fraction of ionic monomers, and colloid charge: $\eta_{Rouse}^{I+} \sim u^{1.34} f^{1.79} Q^{0.89}$ for $\nu = 0.588$. When the chain length exceeds

$$N_{Rouse/rep} \simeq N_e (u^3 f^4 Q^2)^{-1/(4-3\nu)} \tag{B19}$$

topological entanglements between the PEs become substantial, and the reptation mechanism of chain diffusion sets in. For long PEs, the viscosity

$$\eta_{rep}^{I+} \simeq \eta_s (u^3 f^4 Q^2)^{3/(4-3\nu)} \frac{N^3}{N_e^2} \tag{B20}$$

increases very strongly with increasing u, f, and Q: $\eta_{rep}^{I+} \sim u^{4.03} f^{5.37} Q^{2.68}$ for $\nu = 0.588$. The diffusion coefficients for unentangled and entangled diffusion of the colloids, respectively, are equal to[55]

$$D_{np}^{unent} \simeq D_0 {\phi_{I+}}^{-2\nu/(3\nu-1)} R^{-3} \simeq D_0 (u^3 f^4 Q^2)^{-2\nu/(4-3\nu)} R^{-3} \tag{B21}$$

$$D_{np}^{ent} \simeq D_0 {\phi_{I+}}^{-3/(3\nu-1)} R^{-1} {N_e}^2 N^{-3} \simeq D_0 (u^3 f^4 Q^2)^{-3/(4-3\nu)} R^{-1} {N_e}^2 N^{-3} \tag{B22}$$

We emphasize that eqs B19, B20, and B22 are only applicable to an athermal solvent and are not applicable for a Θ solvent; at $\nu = 1/2$, they *do not reduce* to eqs 81, 83, and 90 which are valid for a Θ solvent. This nonuniversality of the scaling predictions for reptation dynamics is caused by different renormalization of the tube diameter in Θ and athermal semidilute solutions.[52,53] In athermal solvent, both structural and dynamical properties of the system are controlled by two-body interactions, which are responsible for both short-range repulsions and topological entanglements. In contrast, for Θ solvent conditions, three-body interactions define the structural (equilibrium) properties, while the reptation tube diameter is still defined by two-body contacts.[53] For this reason, the result for Rouse dynamics remains universal, eqs B18 and B21 reduce to eqs 80 and 85 at $\nu = 1/2$, while the scaling laws for dynamics and colloid mobility in entangled systems do not.

In the regimes of quasi-planar adsorption, II+ and III+, viscoelastic properties are expected to substantially depend on the nanoparticle component of the system.

APPENDIX C

C. Second Virial Coefficient of Interactions between Neutral Colloid−Polyelectrolyte Pairs

We consider the solution of colloid−PE pairs in regime I at $c \gg c_{ads}^I$. To calculate the second virial coefficient of interactions between the neutral pairs, B_{np}, we follow the method of ref 39 and approximate the pairwise interaction potential by the following function:

$$U_{12}(r) = \begin{cases} +\infty & \text{for} \quad r \le H_I - \xi_e \\ F_{br}^I & \text{for} \quad H_I - \xi_e \le r \le H_I \\ 0, & \text{for} \quad r \ge H_I \end{cases} \tag{C1}$$

This shape of $U_{12}(r)$ takes into account weak attractions due to bridging when shells are in contact, $F_{br}^I < 0$, and their strong repulsions at the substantial overlap. The second virial coefficient

$$B_{np}^I \simeq \int_0^\infty (1 - e^{-U_{12}(r)/k_BT}) d^3r \simeq {H_I}^3 \left(1 - \frac{\xi_e}{H_I} e^{H_I/\xi_e}\right) \simeq -\xi_e {H_I}^2 e^{H_I/\xi_e} \tag{C2}$$

Table B1. Structural Properties of the Hybrid Coacervate in Athernal Solvent: Scaling Laws for (i) the Thickness of the Adsorbed Layer, H; (ii) Average Polymer Density within the Shell, ϕ; (iii) Coacervate Surface Tension γ[a]

regime	adsorption type	H	ϕ	γ
I+	strong spherical	$u^{-0.34} f^{-0.79} Q^{0.11}$	$u^{1.03} f^{1.37} Q^{0.68}$	$u^{0.76} f^{1.62} Q^{-0.11}$
II+	strong quasi-planar	$u^{-0.43} f^{-1} Q^{0.13} R^{-0.27}$	$u^{0.43} Q^{0.87} R^{-1.73}$	$u^{0.42} f^{0.83} R^{-1}$
III+	weak quasi-planar	$u^{-0.37} f^{-0.42} Q^{-0.33} R^{0.67}$	$u^{0.37} f^{-0.58} Q^{1.33} R^{-2.67}$	$u^{0.25} f^{-0.83} Q^{1.33} R^{-3.67}$

[a]The numerical values of the exponents are calculated for $\nu = 0.588$.

https://doi.org/10.1021/acs.macromol.2c02464
Macromolecules 2023, 56, 1713−1730

is negative because $H_I \gg \xi_e$ in regime I, so that bridging attractions dominate hard-core repulsions.

To consider the stability of the solution of neutral pairs, one should construct the free energy density as the function of the neutral pairs' concentration, c:

$$\mathcal{F} = c \ln c + B_{np}c^2 + C_{np}c^3 \tag{C3}$$

Here the first term takes into account the translational entropy of the neutral pairs and the second one accounts for their pairwise attractions. The last contribution is the next term in the virial expansion, which takes into account three-body repulsions with $C_{np} \simeq H_I^6$, is added to stabilize (the finite concentration of) the condensed phase. Since we neglect the higher-order repulsions between the pairs, eq C3 cannot provide an accurate description of the condensed phase. However, it enables calculating the solution spinodal in the range of very low concentrations:

$$\frac{d^2\mathcal{F}}{dc^2} = \frac{1}{c} - 2B_{np} + 6C_{np}c\Big|_{c\to 0} \approx \frac{1}{c} - 2B_{np} \tag{C4}$$

The solution becomes unstable with respect to the macroscopic phase separation at

$$c^I_{coac,sp} \simeq -B_{np}^{-1} \simeq e^{-H_I/\xi_e} \simeq e^{-(Q/q_e)^{1/5}} \tag{C5}$$

As in Section 5, we omitted the pre-exponential factor because even the exponents (i.e, the free energies) within the scaling approach are calculated up to the numerical coefficients. The obtained result is consistent with the threshold coacervation concentration, c^I_{coac}, which is given by eq 61. We should note that the threshold concentrations found using binodal and spinodal calculations, $\ln c^I_{coac} \simeq \ln c^I_{coac,sp}$, do not imply that these values are *exactly* equal to each other. Generally speaking, they are unequal, which can be demonstrated using a more refined analysis. The result similar to eq C5 has been recently reported for the spinodal concentration in the case of conventional PE−PE complex coacervation,[43] which is also preceded by the formation of finite-size neutral pairs (globules).[40−42]

Similar reasoning applied to regimes II and III yields

$$B^{II}_{np} \simeq R^3\left(1 - \frac{\xi_e}{R}e^{R/\xi_e}\right) \simeq -\xi_e R^2 e^{R/\xi_e} \tag{C6}$$

$$B^{III}_{np} \simeq R^3\left(1 - \frac{H_{III}}{R}e^{(Q/q_q)^{4/3}(\xi_e/R)^{5/3}}\right) \simeq -H_{III}R^2 e^{(Q/q_q)^{4/3}(\xi_e/R)^{5/3}} \tag{C7}$$

and the respective threshold concentrations, $c^{II}_{coac,sp.}$ and $c^{III}_{coac,sp}$, are in agreement with to the results of eqs 62 and 63.

AUTHOR INFORMATION

Corresponding Authors

Artem M. Rumyantsev − *Pritzker School of Molecular Engineering, University of Chicago, Chicago, Illinois 60637, United States;* orcid.org/0000-0002-0339-2375; Email: rumyantsev@uchicago.edu

Oleg V. Borisov − *Institut des Sciences Analytiques et de Physico-Chimie pour l'Environnement et les Matériaux, UMR 5254 CNRS UPPA, Pau 64053, France;* orcid.org/0000-0002-9281-9093; Email: oleg.borisov@univ-pau.fr

Juan J. de Pablo − *Pritzker School of Molecular Engineering, University of Chicago, Chicago, Illinois 60637, United States;* orcid.org/0000-0002-3526-516X; Email: depablo@uchicago.edu

Complete contact information is available at: https://pubs.acs.org/10.1021/acs.macromol.2c02464

Notes

The authors declare no competing financial interest.

ACKNOWLEDGMENTS

We are grateful to Ekaterina Zhulina and Abhinendra Singh for the helpful discussions. This work is supported by the Department of Energy, Basic Energy Sciences, Division of Materials Science and Engineering. Additional support for the design of complex coacervates for industrial applications is provided by the U.S. Department of Commerce, National Institute of Standards and Technology (NIST), as part of the Center for Hierarchical Materials Design (CHiMaD). O.V.B. acknowledges support by the ANR-DFG TOPOL Project ANR-20-CE92-0044.

REFERENCES

(1) Rumyantsev, A. M.; Jackson, N. E.; de Pablo, J. J. Polyelectrolyte complex coacervates: Recent developments and new frontiers. *Annu. Rev. Condens. Matter Phys.* **2021**, *12*, 155−176.

(2) Sing, C. E.; Perry, S. L. Recent progress in the science of complex coacervation. *Soft Matter* **2020**, *16*, 2885−2914.

(3) Dubin, P. L.; Ross, T. D.; Sharma, I.; Yegerlehner, B. E. Coacervation of polyelectrolyte-protein Complexes. In *Ordered Media in Chemical Separations*; Hinze, W. L., Armstrong, D. W., Eds.; ACS: Washington, DC, 1987; *9*, 162−169.

(4) Kizilay, E.; Kayitmazer, A. B.; Dubin, P. L. Complexation and coacervation of polyelectrolytes with oppositely charged colloids. *Adv. Colloid Interface Sci.* **2011**, *167*, 24−37.

(5) Comert, F.; Dubin, P. L. Liquid-liquid and liquid-solid phase separation in protein-polyelectrolyte systems. *Adv. Colloid Interface Sci.* **2017**, *239*, 213−217.

(6) Comert, F.; Malanowski, A. J.; Azarikia, F.; Dubin, P. L. Coacervation and precipitation in polysaccharide−protein systems. *Soft Matter* **2016**, *12*, 4154−4161.

(7) Klemmer, K. J.; Waldner, L.; Stone, A.; Low, N. H.; Nickerson, M. T. Complex coacervation of pea protein isolate and alginate polysaccharides. *Food Chem.* **2012**, *130*, 710−715.

(8) Wang, Q.; Schlenoff, J. B. The polyelectrolyte complex/coacervate continuum. *Macromolecules* **2014**, *47*, 3108−3116.

(9) Kapelner, R. A.; Yeong, V.; Obermeyer, A. C. Molecular determinants of protein-based coacervates. *Curr. Opin. Colloid Interface Sci.* **2021**, *52*, 101407.

(10) Cummings, C. S.; Obermeyer, A. C. Phase separation behavior of supercharged proteins and polyelectrolytes. *Biochemistry* **2018**, *57*, 314−323.

(11) Yeong, V.; Werth, E. G.; Brown, L. M.; Obermeyer, A. C. Formation of biomolecular condensates in bacteria by tuning protein electrostatics. *ACS Cent. Sci.* **2020**, *6*, 2301−2310.

(12) Kapelner, R. A.; Obermeyer, A. C. Ionic polypeptide tags for protein phase separation. *Chem. Sci.* **2019**, *10*, 2700−2707.

(13) Kim, S.; Sureka, H. V.; Kayitmazer, A. B.; Wang, G.; Swan, J. W.; Olsen, B. D. Effect of protein surface charge distribution on protein-polyelectrolyte complexation. *Biomacromolecules* **2020**, *21*, 3026−3037.

(14) Neitzel, A. E.; Fang, Y. N.; Yu, B.; Rumyantsev, A. M.; de Pablo, J. J.; Tirrell, M. V. Polyelectrolyte complex coacervation across a broad range of charge densities. *Macromolecules* **2021**, *54*, 6878−6890.

(15) Huang, J.; Laaser, J. E. Charge density and hydrophobicity-dominated regimes in the phase behavior of complex coacervates. *ACS Macro Lett.* **2021**, *10*, 1029−1034.

(16) Chang, L.-W.; Lytle, T. K.; Radhakrishna, M.; Madinya, J. J.; Vélez, J.; Sing, C. E.; Perry, S. L. Sequence and entropy-based control of complex coacervates. *Nature Commun.* **2017**, *8*, 1273.
(17) Rumyantsev, A. M.; Jackson, N. E.; Yu, B.; Ting, J. M.; Chen, W.; Tirrell, M. V.; de Pablo, J. J. Controlling complex coacervation via random polyelectrolyte sequences. *ACS Macro Lett.* **2019**, *8*, 1296−1302.
(18) Samanta, R.; Ganesan, V. Influence of protein charge patches on the structure of protein−polyelectrolyte complexes. *Soft Matter* **2018**, *14*, 9475−9488.
(19) Samanta, R.; Halabe, A.; Ganesan, V. Influence of charge regulation and charge heterogeneity on complexation between polyelectrolytes and proteins. *J. Phys. Chem. B* **2020**, *124*, 4421−4435.
(20) Samanta, R.; Ganesan, V. Direct simulations of phase behavior of mixtures of oppositely charged proteins/nanoparticles and polyelectrolytes. *J. Phys. Chem. B* **2020**, *124*, 10943−10951.
(21) Madinya, J. J.; Sing, C. E. Hybrid field theory and particle simulation model of polyelectrolyte−surfactant coacervation. *Macromolecules* **2022**, *55*, 2358−2373.
(22) Rumyantsev, A. M.; Zhulina, E. B.; Borisov, O. V. Complex Coacervate of Weakly Charged Polyelectrolytes: Diagram of States. *Macromolecules* **2018**, *51*, 3788−3801.
(23) Rubinstein, M.; Liao, Q.; Panyukov, S. Structure of liquid coacervates formed by oppositely charged polyelectrolytes. *Macromolecules* **2018**, *51*, 9572−9588.
(24) Aponte-Rivera, C.; Rubinstein, M. Dynamic coupling in unentangled liquid coacervates formed by oppositely charged polyelectrolytes. *Macromolecules* **2021**, *54*, 1783−1800.
(25) Borisov, O. V.; Zhulina, E. B.; Birshtein, T. M. Polyelectrolyte molecule conformation near a charged surface. *J. Phys. France II* **1994**, *4*, 913−929.
(26) Borukhov, I.; Andelman, D.; Orland, H. Scaling laws of polyelectrolyte adsorption. *Macromolecules* **1998**, *31*, 1665−1671.
(27) Dobrynin, A. V.; Deshkovski, A.; Rubinstein, M. Adsorption of polyelectrolytes at an oppositely charged surface. *Phys. Rev. Lett.* **2000**, *84*, 3101−3104.
(28) Dobrynin, A. V.; Deshkovski, A.; Rubinstein, M. Adsorption of polyelectrolytes at oppositely charged surfaces. *Macromolecules* **2001**, *34*, 3421−3436.
(29) Dobrynin, A. V.; Rubinstein, M. Theory of polyelectrolytes in solutions and at surfaces. *Prog. Polym. Sci.* **2005**, *30*, 1049−1118.
(30) de Gennes, P.-G.; Pincus, P.; Velasco, R. M.; Brochard, F. Remarks on polyelectrolyte conformation. *J. Phys. (Paris)* **1976**, *37*, 1461−1473.
(31) Netz, R. R.; Joanny, J.-F. Adsorption of semiflexible polyelectrolytes on charged planar surfaces: Charge compensation, charge reversal, and multilayer formation. *Macromolecules* **1999**, *32*, 9013−9025.
(32) Gurovitch, E.; Sens, P. Adsorption of polyelectrolyte onto a colloid of opposite charge. *Phys. Rev. Lett.* **1999**, *82*, 339−342.
(33) Mateescu, E. M.; Jeppesen, C.; Pincus, P. Overcharging of a spherical macroion by an oppositely charged polyelectrolyte. *Europhys. Lett.* **1999**, *46*, 493−498.
(34) Gelbart, W. M.; Bruinsma, R. F.; Pincus, P. A.; Parsegian, V. A. DNA-inspired electrostatics. *Phys. Today* **2000**, *53*, 38−44.
(35) Jonsson, M.; Linse, P. Polyelectrolyte−macroion complexation. I. Effect of linear charge density, chain length, and macroion charge. *J. Chem. Phys.* **2001**, *115*, 3406−3418.
(36) de Gennes, P. G. Polymers at an interface: A simplified view. *Adv. Colloid Interface Sci.* **1987**, *27*, 189−209.
(37) Bonet Avalos, J.; Johner, A.; Joanny, J. F. Bridging by adsorbed polymers between two surfaces. *J. Chem. Phys.* **1994**, *101*, 9181−9194.
(38) Semenov, A. N.; Joanny, J.-F.; Khokhlov, A. R. Associating polymers: Equilibrium and linear viscoelasticity. *Macromolecules* **1995**, *28*, 1066−1075.
(39) Borisov, O. V.; Halperin, A. Micelles of polysoaps: The role of bridging interactions. *Macromolecules* **1996**, *29*, 2612−2617.
(40) Rumyantsev, A. M.; Potemkin, I. I. Explicit description of complexation between oppositely charged polyelectrolytes as an advantage of the random phase approximation over the scaling approach. *Phys. Chem. Chem. Phys.* **2017**, *19*, 27580−27592.
(41) Delaney, K. T.; Fredrickson, G. H. Theory of polyelectrolyte complexation — Complex coacervates are self-coacervates. *J. Chem. Phys.* **2017**, *146*, 224902.
(42) Zhang, P.; Wang, Z.-G. Supernatant phase in polyelectrolyte complex coacervation: Cluster formation, binodal, and nucleation. *Macromolecules* **2022**, *55*, 3910−3923.
(43) Chen, S.; Wang, Z.-G. Driving force and pathway in polyelectrolyte complex coacervation. *Proc. Natl. Acad. Sci. U.S.A.* **2022**, *119*, No. e2209975119.
(44) Shusharina, N. P.; Zhulina, E. B.; Dobrynin, A. V.; Rubinstein, M. Scaling theory of diblock polyampholyte solutions. *Macromolecules* **2005**, *38*, 8870−8081.
(45) Semenov, A. N.; Joanny, J.-F.; Johner, A.; Bonet Avalos, J. Interaction between two adsorbing plates: The effect of polymer chain ends. *Macromolecules* **1997**, *30*, 1479−1489.
(46) Borisov, O. V. Conformations of star-branched polyelectrolytes. *J. Phys. France II* **1996**, *6*, 1−19.
(47) Leermakers, F. A. M.; Ballauff, M.; Borisov, O. V. Counterion localization in solutions of starlike polyelectrolytes and colloidal polyelectrolyte brushes: A self-consistent field theory. *Langmuir* **2008**, *24*, 10026−10034.
(48) Tang, Q.; Rubinstein, M. Where in the world are condensed counterions? *Soft Matter* **2022**, *18*, 1154−1173.
(49) Borisov, O. V.; Halperin, A. Micelles of polysoaps. *Langmuir* **1995**, *11*, 2911−2919.
(50) Danielsen, S. P. O.; Panyukov, S.; Rubinstein, M. Ion pairing and the structure of gel coacervates. *Macromolecules* **2020**, *53*, 9420−9442.
(51) Rumyantsev, A. M.; Johner, A.; Tirrell, M. V.; de Pablo, J. J. Unifying weak and strong charge correlations within the random phase approximation: Polyampholytes of various sequences. *Macromolecules* **2022**, *55*, 6260.
(52) Rubinstein, M.; Colby, R. H. *Polymer Physics*; Oxford University Press, 2003.
(53) Colby, R. H.; Rubinstein, M. Two-parameter scaling for polymers in Θ solvents. *Macromolecules* **1990**, *23*, 2753−2757.
(54) Brochard Wyart, F.; de Gennes, P. G. Viscosity at small scales in polymer melts. *Eur. Phys. J. E* **2000**, *1*, 93−97.
(55) Cai, L.-H.; Panyukov, S.; Rubinstein, M. Mobility of nonsticky nanoparticles in polymer liquids. *Macromolecules* **2011**, *44*, 7853−7863.
(56) Cai, L.-H.; Panyukov, S.; Rubinstein, M. Hopping diffusion of nanoparticles in polymer matrices. *Macromolecules* **2015**, *48*, 847−862.
(57) Yu, B.; Rauscher, P. M.; Jackson, N. E.; Rumyantsev, A. M.; de Pablo, J. J. Crossover from Rouse to reptation dynamics in salt-free polyelectrolyte complex coacervates. *ACS Macro Lett.* **2020**, *9*, 1318−1324.
(58) Brady, J. F. The rheological behavior of concentrated colloidal dispersions. *J. Chem. Phys.* **1993**, *99*, 567−581.
(59) Verberg, R.; de Schepper, I. M.; Cohen, E. G. D. Viscosity of colloidal suspensions. *Phys. Rev. E* **1997**, *55*, 3143−3158.
(60) Cohen, E. G. D.; Verberg, R.; de Schepper, I. M. Viscosity and diffusion in hard-sphere-like colloidal suspensions. *Phys. A* **1998**, *251*, 251−265.
(61) Schweizer, K. S.; Saltzman, E. J. Entropic barriers, activated hopping, and the glass transition in colloidal suspensions. *J. Chem. Phys.* **2003**, *119*, 1181−1196.
(62) Dobrynin, A. V. Effect of solvent quality on polyelectrolyte adsorption at an oppositely charged surface. *J. Chem. Phys.* **2001**, *114*, 8145−8153.

https://doi.org/10.1021/acs.macromol.2c02464
Macromolecules 2023, 56, 1713−1730